

## RESSALVA

Atendendo solicitação do(a) autor(a), o texto completo desta tese será disponibilizado somente a partir de 23/10/2025.

# THÈSE

*présentée à*

**L'UNIVERSITÉ DE BORDEAUX**

**École Doctorale des Sciences Chimiques**

*et*

**L'UNIVERSIDADE ESTADUAL PAULISTA**

**“JÚLIO DE MESQUITA FILHO”**

**Instituto de Química – *campus* Araraquara**

*par*

**Leonardo Vieira ALBINO**

pour obtenir le titre de

**DOCTEUR**

**Spécialité: Chimie ET Physico-chimie de la matière condensée**

\*\*\*\*\*

**Synthèse et étude de verres à propriétés magnéto-optiques  
contenant des métaux de transition et des terres rares**

\*\*\*\*\*

**Soutenue le 23 octobre 2023**

Membres du jury :

**M. NALIN Marcelo, Professor**

de Mesquita Filho » *campus* Araraquara (IQ-UNESP)

**M. CARDINAL Thierry, Docteur**

Université de Bordeaux (ICMCB-UB)

**M. DUCLERE Jean-René, Professor**

Limoges (IRCER-UL)

**M. POIRIER Gael-Yves, Professor**

Alfenas *campus* Poços de Caldas (ICT-UNIFAL-MG)

**Mme GONÇALVES Rogéria Rocha, Professeure**

Universidade de São Paulo (FFCLRP-USP)

Instituto de Química – Universidade Estadual Paulista « Júlio

– **Directeur de thèse**

Institut de Chimie de la Matière Condensée de Bordeaux –

– **Directeur de thèse**

Institut de Recherche sur les Céramiques – Université de

– **Rapporteur**

Instituto de Ciência e Tecnologia – Universidade Federal de

– **Rapporteur**

Faculdade de Filosofia, Ciências e Letras de Ribeirão Preto -

– **Examineur & Président du Jury**

A336s Albino, Leonardo Vieira  
Síntese e estudo de vidros magneto-ópticos contendo metais de transição e terras raras / Leonardo Vieira Albino – Araraquara: [s.n.], 2023  
203 p.: il.

Tese (doutorado) – Universidade Estadual Paulista, Instituto de Química  
Orientador: Marcelo Nalin  
Coorientador: Thierry Cardinal  
Coorientador: Sidney José Lima Ribeiro

1. Vidro. 2. Magnetoptica. 3. Efeito de Faraday.  
4. Metais de terras raras. 5. Manganês. I. Título.

Sistema de geração automática de fichas catalográficas da Unesp. Biblioteca do Instituto de Química, Araraquara. Dados fornecidos pelo autor(a).

Essa ficha não pode ser modificada



---

Leonardo Vieira Albino

# **Síntese e Estudo de Vidros Magneto-Ópticos contendo Metais de Transição e Terras Raras**

Tese em cotutela apresentada ao Instituto de Química, Universidade Estadual Paulista “*Júlio de Mesquita Filho*” (IQ/UNESP) e Institut de Chimie de la Matière Condensée de Bordeaux, Université de Bordeaux (ICMCB/UB) para obtenção do título de Doutor em Química, especialidade em Físico-Química da Matéria Condensada

Orientador: Prof. Dr. Marcelo Nalin

Coorientador: Dr. Thierry Cardinal

Coorientador: Prof. Dr. Sidney José Lima Ribeiro

**Araraquara**

**2023**

---

## Impacto potencial da pesquisa

Vidros com aplicações magneto-ópticas vem se tornando cada vez mais procurados por pesquisadores e empresas, sendo uma promessa significativa para vários avanços tecnológicos, com impactos potenciais que abrangem diversos setores. Em primeiro lugar, a exploração destes vidros pode impulsionar as tecnologias de comunicação. Os rotadores Faraday, dispositivos que giram a polarização da luz na presença de um campo magnético, são componentes integrais em sistemas de comunicação óptica. Ao melhorar as propriedades magneto-ópticas dos vidros, os pesquisadores podem abrir caminho para redes de comunicação óptica mais eficientes e rápidas. Isto poderia levar a melhores taxas de transmissão de dados, redução de perdas de sinal e aumento de largura de banda, atendendo à crescente demanda por comunicações mais rápidas e confiáveis. Também tem implicações profundas para o desenvolvimento de tecnologias de sensoriamento. As propriedades magneto-ópticas desses vidros podem ser aproveitadas na criação de sensores magnéticos/elétricos altamente sensíveis. Esses sensores podem encontrar aplicações em diversos campos, incluindo diagnósticos médicos, monitoramento ambiental e processos industriais. Atualmente vidros magneto-ópticos apresentam-se como um possível substituto dos monocristais utilizados comercialmente, devido as características isotrópicas, o processo de produção mais simples e a possibilidade de produção de fibras ópticas. Para esse fim, várias matrizes vítreas que suportem altas concentrações de terras-raras sem induzir cristalização vem sendo sintetizadas e estudadas. Vidros borogermanato vem se mostrando uma boa alternativa, porém os reagentes e a síntese desses vidros elevam o custo. Esta tese de doutorado teve como objetivo sintetizar e caracterizar diferentes sistemas vítreos mais baratos, um borotungstato contendo terras-raras e outro fosfato contendo manganês visando obter respostas magnéticas próximas aos monocristais e vidros germanato comerciais.

---

## Potential research impact

Glasses with magneto-optical applications have become increasingly sought after by researchers and companies, holding significant promise for various technological advances, with potential impacts that span diverse sectors. Firstly, the exploration of these glasses can boost communication technologies. Faraday rotators, devices that rotate the polarization of light in the presence of a magnetic field, are integral components in optical communication systems. By improving the magneto-optical properties of glasses, researchers can pave the way for more efficient and faster optical communication networks. This could lead to better data transmission rates, reduced signal losses and increased bandwidth, addressing the ever-growing demand for faster and more reliable communication. Moreover, the research has profound implications for the development of advanced sensing technologies. The magneto-optical properties of these glasses can be used to create highly sensitive magnetic/electrical sensors. These sensors can find applications in a variety of fields, including medical diagnostics, environmental monitoring, and industrial processes. Currently, magneto-optical glasses are a possible replacement for commercially used monocrystals, due to their isotropic characteristics, the simpler production process and the possibility of producing optical fibers. To this end, several glass matrices that support high concentrations of rare earths without inducing crystallization have been synthesized and studied. Borogermanate glasses have proven to be a good alternative, but the reagents and synthesis of these glasses increase the cost. This doctoral thesis aimed to synthesize and characterize different cheaper glass systems, a borotungstate containing rare earths and another phosphate containing manganese, aiming to obtain magnetic responses close to commercial monocrystals and borogermanate glasses.

**CERTIFICADO DE APROVAÇÃO**

TÍTULO DA TESE: "Síntese e Estudo de Vidros Magneto-Ópticos contendo Metais de Transição e Terras Raras"

**AUTOR: LEONARDO VIEIRA ALBINO**

**ORIENTADOR: MARCELO NALIN**

**COORIENTADOR: SIDNEY JOSE LIMA RIBEIRO**

**COORIENTADOR: THIERRY CARDINAL**

Aprovado como parte das exigências para obtenção do Título de Doutor em Química, pela Comissão Examinadora:



Prof. Dr. MARCELO NALIN (Participação Presencial)  
Departamento de Química Analítica, Físico-Química e Inorgânica / Instituto de Química - UNESP - Araraquara

Prof. Dr. THIERRY CARDINAL (Participação Virtual)  
Institut de Chimie de la Matière Condensée de Bordeaux - UB - França

Prof. Dr. GAEL YVES POIRIER (Participação Presencial)  
Instituto de Ciência e Tecnologia / Universidade Federal de Alfenas - UNIFAL - Poços de Caldas

Profa. Dra. ROGÉRIA ROCHA GONÇALVES (Participação Virtual)  
Departamento de Química / Faculdade de Filosofia Ciências e Letras - USP - Ribeirão Preto

Prof. Dr. JEAN-RENÉ DUCLÉRE (Participação Virtual)  
Institut de Recherche sur les Céramiques / Université de Limoges - França

Araraquara, 23 de outubro de 2023

---

Leonardo Vieira Albino; L. V. Albino; L. V. ALBINO

### **Occupation area**

Major Area: Exact and Earth Sciences / Area: Chemistry / Subarea: Inorganic Chemistry.

Major Area: Exact and Earth Sciences / Area: Chemistry / Subarea: Materials Chemistry.

Major Area: Exact and Earth Sciences / Area: Chemistry / Subarea: Non-Crystalline Materials Chemistry.

### **Personal information**

Birth date: January 21, 1994 - 29 years

Nationality: Brazilian.

Place of birth: Itapetininga, SP, Brazil.

Affiliation: Marcos Antônio Albino and Patrícia Maria Diniz Vieira Albino.

Marital status: single.

Occupation: PhD student.

Email: [leonardoalbino63@gmail.com](mailto:leonardoalbino63@gmail.com)

Curriculo Lattes (in Portuguese): <http://lattes.cnpq.br/0124534306474504>

ORCID iD: <https://orcid.org/0000-0003-0441-2371>

### **Professional address**

São Paulo State University (UNESP), Institute of Chemistry, Department of General and Inorganic Chemistry, Laboratório de Vidros Especiais (LaViE).

Av. Prof. Francisco Degni, 55

Jardim Quitandinha

14800060 - Araraquara, SP, Brazil

Telephone: +55 (16) 33019654

---

## Academic education

**PhD in Physico-Chimie de la Matière Condensée in progress.** 2021 – in progress.

Institut de Chimie de la Matière Condensée de Bordeaux (ICMCB), UMR5026, CNRS, University of Bordeaux (UB) and Bordeaux INP.

Advisor: Dr. Thierry Cardinal

Scholarship: FUNGlass, received funding from the European Union's Horizon 2020 research and innovation programme under the Marie Skłodowska-Curie grant agreement No 823941.

**PhD in Chemistry in progress** (grade CAPES 7). 2018 – in progress

São Paulo State University (UNESP), Institute of Chemistry, Department of General and Inorganic Chemistry, Laboratório de Vidros Especiais (LaViE).

Title of thesis: Synthesis and Study of Magneto-Optic Glasses containing Transition Metals and Rare Earths.

Advisor: Prof. Dr. Marcelo Nalin.

Co-advisor: Prof. Dr. Sidney José Lima Ribeiro.

Scholarship: Coordenação de Apoio a Pesquisa no Ensino Superior (CAPES), Brazil.

**Master in Chemistry** (grade CAPES 7). 2016 - 2018

São Paulo State University (UNESP), Institute of Chemistry, Department of General and Inorganic Chemistry, Laboratório de Vidros Especiais (LaViE).

Title of dissertation: Study, Preparation and Application of Polymeric Optical Fibers using 3D Printing technology.

Advisor: Marcelo Nalin.

Scholarship: Coordination for the Improvement of Higher Education Personnel (CAPES), Brazil.

**Bachelor in Chemistry.** 2012 - 2015

São Paulo State University (UNESP), Institute of Chemistry, Department of General and Inorganic Chemistry, Laboratório de Vidros Especiais (LaViE).

---

Title of coursework completion: Luminescent Properties of Europium and Copper Doped PbO-GeO<sub>2</sub> Glass.

Advisor: Marcelo Nalin.

Scholarship: São Paulo Research Foundation (FAPESP), Brazil.

**Technical/Professionalizing course in Chemistry.** 2010 - 2011

Salles Gomes State Technical School (Paula Souza Center). Tatuí, Brazil.

### **Additional education**

**Minicourse Lanthanides: Chemistry, Luminescence and Applications**, by Prof. Dr. Fernando Aparecido Sigoli. (Hours: 6). 46th Annual Meeting of the Brazilian Society of Chemistry (RASBQ). Águas de Lindóia - Brazil. (2023)

**MOOC - Intégrité scientifique dans les métiers de la recherche.** Université de Bordeaux. (2023)

**French language course. Niveau B2 - Evening - Département d'Etudes de Français Langue Etrangère (DEFLE).** (Hours: 50). Université Bordeaux-Montaigne, France. (2022)

**2nd ICG-CGCRI Tutorial 2021 on Glass Science & Technology** hosted by CSIR - Central Glass & Ceramic Research Institute, Kolkata - India, in association with International Commission on Glass, from 18th to 27th January - online (2021)

**Pedagogical Training Workshop: Dialogues on University Teaching - PPD/FCF and Program for the Improvement and Support of Teaching in Higher Education (PAADES) - Campus** (Hours: 8). São Paulo State University (UNESP), Brazil. (2019)

**Pedagogical Training Workshop - Program for the Improvement and Support of Teaching in Higher Education (PAADES).** (Hours: 22). São Paulo State University (UNESP), Brazil. (2018)

**Introduction to 3D modeling of free software.** (Hours: 15). Araraquara University (UNIARA), Brazil. (2016)

**Next generation gene arrays: fresh new tools for.** (Hours: 1). AFFYMETRIX BIOTECH LTDA, AB\_FORN, Brazil. (2014)

---

**Web of Science, EndNote e ResearcherID.** Thomson Reuters Serviços Econômicos, THOMSON REUTERS, Brazil. (2014)

**Forensic Medical Sciences.** Courses and Events Renova, RENOVA CURSOS, Brazil. (2013)

### **Professional Experience**

1. **Professor of Experimental Inorganic Chemistry** for the Chemical Engineering course (2019) by the Program for the Improvement and Support of Teaching in Higher Education (PAADES). São Paulo State University (UNESP), Institute of Chemistry, Araraquara, Brazil. (2019). 64h.
2. **Professor of General and Inorganic Chemistry I** for the Pharmacy-Biochemistry course (evening–2019) by the Program for the Improvement and Support of Teaching in Higher Education (PAADES). São Paulo State University (UNESP), Institute of Chemistry, Araraquara, Brazil. (2019). 64h.
3. **Intervention activity in the General Chemistry Laboratory** discipline for 1st year students of the Chemical Engineering course by the Special Topics discipline: Chemistry Teaching Practice - Theory and experiment. São Paulo State University (UNESP), Institute of Chemistry, Araraquara, Brazil. (2017). 180h.
4. **Teaching practice in Experimental Inorganic Chemistry** for Licentiate in chemistry students (2013) offered by the Coordination for the Improvement of Higher Education Personnel (CAPES) and Department of General and Inorganic Chemistry, São Paulo State University (UNESP), Institute of Chemistry, Araraquara, Brazil. (2017). 60h.
5. **Monitor of the General Physical Chemistry** discipline for Bachelor in chemistry (2013) offered by the Department of Physical Chemistry and Tutorial Education Program in Chemistry (PET-Química). São Paulo State University (UNESP), Institute of Chemistry, Araraquara, Brazil. (2013). 60h.
6. **Ministered short course Workshop: Origin**, during the XLIII Chemistry Week. São Paulo State University (UNESP), Institute of Chemistry, Araraquara, Brazil. (2013). 2h.

---

## Languages

### Portuguese

Comprehends Well, Speaks Well, Reads Well, Writes Well.

### English

Comprehends Well, Speaks Well, Reads Well, Writes Reasonably.

### French

Comprehends Well, Speaks Well, Reads Well, Writes Well. Niveau DELF B2.

## Scientific production

### Articles published in scientific journals

D. F. Franco, F. J. Caixeta, L. V. Albino, T. A. Lodi, J. R. Orives, E. O. Ghezzi, M. Nalin, **Terbium-doped transparent glass-ceramics containing TbPO<sub>4</sub> crystals: A promising material for photonic applications**. Opt. Mater. X. 20 (2023) 100272  
<https://doi.org/10.1016/j.omx.2023.100272>

### Presented works

1. Albino, L. V.; Cardinal, T.; Dussauze, M.; Adamietz, F.; Toulemonde, O.; Jubera, V.; Franco, D. F.; Nalin, M. **“Paramagnetic borotungstate glasses – a new magnetic-optical material”**. 46 RASBQ. Águas de Lindóia - Brazil. (2023)
2. Ghezzi, E. O.; Albino, L. V.; Lodi, T. A.; Franco, D. F.; Nalin, M.; **“Synthesis and characterization of glasses for ultra-sensitive magneto-optical sensors”**. 46 RASBQ. Águas de Lindóia - Brazil. (2023)
3. Albino, L. V.; Cardinal, T.; Dussauze, M.; Adamietz, F.; Toulemonde, O.; Jubera, V.; Franco, D. F.; Nalin, M. **“Estudos de vidros borotungstato com alta concentração de terras raras para aplicação fotônica”**. Reunião Regional do Instituto Nacional de Ciência e Tecnologia de Fotônica (INFO). Ribeirão Preto - Brazil. (2023)
4. Albino, L. V.; Jubera, V.; Cardinal, T.; Toulemonde, O.; Dussauze, M.; Nalin, M. **“Structural, optical and magnetic properties of high rare earths ions containing Borotungstate glasses”**. XX B-MRS Meeting, Foz do Iguaçu - Brazil. (2022)

- 
5. Albino, L. V.; Dussauze, M.; Toulemonde, O.; Jubera, V.; Cardinal, T.; Nalin, M. **“Borotungstate glasses with a high concentration of rare earths for photonic application”**. 26th International Congress on Glass (ICG2022). Berlin - Germany. (2022)
  6. Albino, L. V.; Dussauze, M.; Danto, S.; Canioni, L.; Toulemonde, O.; Jubera, V.; Cardinal, T.; Nalin, M. **“Verre borotungstate d’ions de terres rares: Matériaux magnétiques pour la photonique”** 89e Congrès de l’Acfas. On-line. Oral presentation in french. 2022
  7. Albino, L. V.; Dussauze, M.; Danto, S.; Canioni, L.; Toulemonde, O.; Jubera, V.; Cardinal, T.; Nalin, M. **“Magnetic materials for photonic applications: Borontungstate and rare earth ions glasses”**. Physical Chemistry & Chemical Physics Workshop (PCCP-2022). Université de Bordeaux. Oral presentation in English. 2022
  8. Roque, N. G.; Albino, L. V.; Marcondes, L. M.; Nalin, M. **“Obtenção do sistema vítreo SbPO<sub>4</sub>-ZnO-PbO-MnO e estudo das propriedades térmicas, ópticas e estruturais”**. XXXII UNESP Scientific Initiation Congress (CIC-UNESP). On-line. (2020)
  9. Roque, N. G.; Albino, L. V.; Marcondes, L. M.; Nalin, M. **“Synthesis of the SbPO<sub>4</sub>-ZnO-PbO-MnO magneto-luminescent glasses”**. #LatinXChem Twitter Conference 2020. On-line. (2020)
  10. Albino, L. V.; Nalin, M. **“Synthesis of transparent magneto-luminescent glass-ceramics with high concentrations of Tb<sup>3+</sup>”**. II Workshop National Institute of Photonics (INFo). Araraquara, Brazil. (2020)
  11. Roque, N. G.; Albino, L. V.; Nalin, M. **“Synthesis of the SbPO<sub>4</sub>-ZnO-PbO-MnO magneto-luminescent glass”**. II Workshop National Institute of Photonics (INFo). Araraquara, Brazil. (2020)
  12. Roque, N. G.; Albino, L. V.; Nalin, M. **“Estudo das propriedades térmicas, ópticas e estruturais do sistema vítreo SbPO<sub>4</sub>-ZnO-PbO em função da concentração de MnO”**. XXXI UNESP Scientific Initiation Congress (CIC-UNESP). Araraquara, Brazil. (2019)

- 
13. Ramos, R. G.; Albino, L. V.; Santagneli, S. H. “**Estudo da estrutura e propriedades de vidros boro-fosfato modificados com  $\text{AlF}_3$** ”. XXXI UNESP Scientific Initiation Congress (CIC-UNESP). Araraquara, Brazil. (2019)
  14. Sampaio, A. C. S.; Albino, L. V.; Nalin, M. “**Estudo das propriedades térmicas, ópticas e estruturais do sistema  $\text{La}_2\text{O}_3\text{-B}_2\text{O}_3\text{-WO}_3$  dopados com  $\text{Dy}^{3+}$ ,  $\text{Tb}^{3+}$  e  $\text{Eu}^{3+}$** ”. XXXI UNESP Scientific Initiation Congress (CIC-UNESP). Araraquara, Brazil. (2019)
  15. Sampaio, A. C. S.; Albino, L. V.; Nalin, M. “**Síntese de vidros boro-tungstato com alta concentração de lantânio**”. XXX UNESP Scientific Initiation Congress (CIC-UNESP). Araraquara, Brazil. (2018)
  16. Albino, L. V.; Nalin, M. “**Preparation of Polymeric Optical Fibers using 3D Printing technology and its application as sensors**”. International Conference on Optical, Optoelectronic and Photonic Materials and Applications (ICOOPMA). Maresias, Brazil. (2018)
  17. Albino, L. V.; Nalin, M. “**Preparação de Fibras Ópticas Poliméricas utilizando tecnologia de Impressão 3D**”. 57<sup>o</sup> Brazilian Congress of Chemistry. Gramado, Brazil. (2017)
  18. de Castro, G. B.; Porsani, G. F.; Albino, L. V.; Nalin, M. “**Multicore polymeric optical fiber obtained from preform with 3D printer**”. XXVIII UNESP Scientific Initiation Congress (CIC-UNESP). Araraquara, Brazil. (2016)
  19. Albino, L. V.; Silva, M. C. C.; Nalin, M. “**Estudo das propriedades luminescentes de vidros  $\text{PbO-GeO}_2$  dopados com európio e cobre**”. 38<sup>a</sup> Annual Meeting of the Brazilian Chemical Society. Águas de Lindóia, Brazil. (2015)
  20. Albino, L. V.; Silva, M. C. C.; Nalin, M. “**Estudo das propriedades ópticas dos vidros e vitrocerâmicas  $\text{PbO-GeO}_2$  dopados com európio e cobre**”. XXVII UNESP Scientific Initiation Congress (CIC-UNESP). Araraquara, Brazil. (2015)
  21. dos Santos, I. F. M.; de Jesus, C. A. S.; Albino, L. V.; de Campos, G. P.; Faria, D. V.; Coco, J.; Teixeira, I. S.; Anhesine, N. B.; Rodrigues Júnior, J. R.; Tayar, S. P.; Lopes, M. N. “**Diagnóstico PET do curso de Bacharelado em Química do IQ/UNESP/CAR**”. XVIII National Meeting of PET Groups (ENAPET). Recife, Brazil. (2013)

---

## Participation in Events

Poster evaluation during **XXXII UNESP Scientific Initiation Congress (CIC-UNESP)**. On-line. (2020)

Presentation of “Photonic demonstration experiments: Photophone, Fiber optics and Preform; Total internal reflection; Infrared, red and green lasers” during **Science at School**. Araraquara, Brazil. (2019)

Poster evaluation during **XXXI UNESP Scientific Initiation Congress (CIC-UNESP)**. Araraquara, Brazil. (2019)

Poster evaluation during **XXX UNESP Scientific Initiation Congress (CIC-UNESP)**. Araraquara, Brazil. (2018)

**Symposium in Commemoration of the International Year of Crystallography: Impact of Crystallography in Different Areas of Science**, module I, diffraction and X-ray scattering. (2014)

## Prizes

Best works in the poster session of the Materials Division: Ghezzi, E. O.; Albino, L. V.; Lodi, T. A.; Franco, D. F.; Nalin, M.; “**Synthesis and characterization of glasses for ultra-sensitive magneto-optical sensors**”. 46 RASBQ. Águas de Lindóia - Brazil. (2023)

---

## **Dedication**

*Dedico este trabalho ao meu querido avô **José Benedito** (1942–2020), homem que, mesmo sem pai, tornou-se o melhor pai e avô deste mundo, sendo uma das inúmeras vítimas da COVID-19.*

---

## **Agradecimentos – Acknowledgment – Remerciements**

*A jornada foi longa. Foram onze anos dedicados a viver o sonho de um jovem de 18 anos, feliz por ter passado no vestibular no curso e na cidade que queria. Não fazia ideia da proporção que me levaria no futuro. Não só conhecer e entender como a Ciência funciona e funciona, mas também contribuir para ela. Neste percurso, foram inúmeros os desafios, mas também inúmeros e agradáveis sucessos. Várias, inúmeras pessoas participaram direta ou indiretamente, para o bem ou para o mal, do meu crescimento científico, profissional e pessoal, o que me coloca numa situação difícil não só de nomeá-las todas, mas de garantir que sejam contempladas por esta simples menção.*

*Primeiramente quero agradecer a minha família. Minha âncora. Ao meu pai Marcos, minha mãe Patrícia, minha irmã Cristiane, que me amaram desde que nasci, me incentivaram a ser uma pessoa ética, forte, alegre e humana. Aos meus avós que também nunca desistiram de pensar, orar e fazer tudo ao seu alcance por mim. Aos meus tios, primos e todos os antepassados, que apesar da minha ausência da minha cidade natal, sempre me receberam com sorrisos, gargalhadas, preocupações e acolhimento, fortalecendo-me e enchendo-me de esperança.*

*Não posso deixar de comentar sobre a minha cidade natal, Itapetininga, a qual agradeço por ser a cidade natal de minha família e onde fiz amigas queridas que levarei comigo para toda a vida. Meu salve para vocês Bodão, Wandell, Sonoda, Tiaki, Paulinho e Bruno. Também gostaria de agradecer a meus professores do Ensino Médio, do Instituto Imaculada Conceição – Itapetininga, e do Curso Técnico em Química da Etec Sales Gomes – Tatuí, que me fizeram apaixonar pela Ciência e pela Química.*

*A minha amada República Diretoria, que me acolheu em fevereiro de 2012. Com certeza me ajudou a vencer minha timidez, me deixando um pouco mais responsável e maduro. Obrigado por aguentarem minhas loucuras e darem-me um nome. Um abraço especial para os diretores com quem convivi: Cafundó, Ariel, Jontex, Alfi, Gargamel, Al-Jazeera, Xaveco, Nissin, Fuinha, Bombinha, Dy, Zé, Conrado, Margarida, Jan, Rooney, Féélope, Trepadeira, Matuta, Lalau, Vlad, Bilé, Pipico, Chicabom, DuPai, Hortência, Pupunha, R7, Moiado, Carinhoso, Lírio, Ragnar, Resgate, Bife e DogRagnar. DIRETORIAA ARRUL, ARRUL, ARRUL!!*

*Agradeço ao meu orientador Prof. Dr. Marcelo Nalin (Pre) pela oportunidade de trabalhar em seu laboratório, pelo apoio, pela inspiração, pela paciência e pelos ensinamentos em química, além da confiança depositada em mim nesses 10 anos.*

*A todos integrantes do Laboratório de Vidros Especiais e do Laboratório de Materiais Fotônicos, em especial ao Prof. Sidney, Prof. Douglas, Dra. Silvia, Prof. Edison, Lia, Juliane, Juliana, Samira, Nicole, Antonio Eduardo, Eduardo Ghezzi, Thiago, Adriana, Bea Freitas, Fábio, Léo e Vibra, pelo conhecimento compartilhado, pelas ajudas, ombros amigos e pelas divertidas discussões.*

*Aos funcionários e alunos do Instituto de Química, em especial os professores, por aumentar minha paixão por química no grau de querer futuramente lecionar numa*

---

*universidade. Também à técnica-administrativa Wennia, por todo auxílio durante a cotutela. Obrigado por essa chance que poucos no nosso país têm.*

*This study was financed in part by the Coordenação de Aperfeiçoamento de Pessoal de Nível Superior - Brasil (CAPES) - Finance Code 001 (grant 88887.571031/2020-00 and 88882.330082/2019-01).*

*I would also like to thank the FunGlass Project for funding, from the European Union's Horizon 2020 research and innovation program under the Marie Skłodowska-Curie (grant agreement 823941), to the Center for Research, Technology and Education in Vitreous Materials (FAPESP, grant 2013/07793-6), French National Center for Scientific Research (CNRS), Bordeaux INP and National Council for Scientific and Technological Development (CNPq). Financing and support that allowed me to grow not only professionally, but also personally, socially and culturally.*

*Um agradecimento especial as minhas professoras de línguas, Carla, et surtout Islene, pour la tâche incroyable de m'aider à apprendre la langue française en peu de temps, m'aidant toujours, avec un professionnalisme et une volonté excellents. And Lenita, my English teacher, also for all her understanding, effort and help, for bringing out my dormant "English" and helping me with my greatest difficulties with patience, professionalism and good humor.*

*Aos meus grandes amigos que vou levar para toda a vida, Palmito, Maria, Cartola e Arroyos (Santiago) por todos os momentos alegres nessa caminhada.*

*E ao meu querido Fernando, que conheci no início do doc durante meu café com maçã, por todo companheirismo, amizade, força, conselhos, risadas, acolhimento e amor nos momentos fáceis e terríveis por toda essa minha jornada. Você é incrível!*

*Je n'ai pas pu m'empêcher de remercier tout particulièrement tout le monde en France. D'abord à mon directeur de thèse, M. Dr. Thierry Cardinal, pour l'opportunité de travailler dans son laboratoire, pour le soutien et pour les enseignements formidables et valables.*

*Je ne peux pas non plus oublier de remercier Dr. Marc Dussauze et Prof. Dr. Véronique Jubera, pour son amitié et aussi pour toute sa patience et ses enseignements durant mon séjour à Bordeaux et au-delà.*

*À l'Institut de Chimie de la Matière Condensée de Bordeaux (ICMCB) et à l'Institut des Sciences Moléculaires (ISM) et aux personnes que j'ai rencontrées dans ces laboratoires, pour toute l'aide et la structure. Je remercie les professionnels Sylvain Danto, Olivier Toulemonde, Patrick Rosa, Mattieu Duttine et Alexandre Fargues, Fred Adamietz, Vincent Rodriguez, Christian Aupetit et, en particulier, mes amis William, Gislene, Ana, Janete, Georges, Florian, Rayan, Fouad, Alizée, Louis, Sara, Mikko, Romain, Simon, Samar, Shashank, Alice, Julia, Lara, Clara, Simon, pour la convivialité à l'intérieur et à l'extérieur du laboratoire.*

*I hope I have reached as many people as possible. You were part of the construction of this work and of this person who speaks to you. No one can win alone!*

***If I have seen further it is by standing on the shoulders of Giants***

---

*Quando a educação não é libertadora, o sonho do oprimido é ser o opressor.*

*When education is not liberating, the dream of the oppressed is to be the oppressor.*

*Quand l'éducation n'est pas libératrice, le rêve de l'opprimé est d'être l'opresseur.*

Paulo Freire (1921–1997)

Citação atribuída a Paulo Freire no livro “*Começando bem, frases e pensamentos*”, de Carlos H. Biagolini (2009).  
A frase não está presente na obra “*Pedagogia do oprimido*”, trata-se de um resumo das ideias do autor

---

## Resumo

O estudo e preparação de novos materiais magneto-ópticos tem ganhado atenção significativa devido às suas potenciais aplicações em vários domínios tecnológicos. Vidros que suportam altas concentrações de íons paramagnéticos estão sendo muito procurados para esses fins, devido às propriedades inerentes que podem ser impostas aos vidros como alta janela de transmissão, altos índices de refração, fácil síntese e modelagem, todas propriedades interessantes para sistemas ópticos e inerente isotropia. Esta tese de doutorado investiga o domínio da ciência de materiais, investigando a síntese e ampla caracterização de dois sistemas vítreos, um borotungstato contendo primeiro térbio e posteriormente um estudo estendido a outros lantanídeos, e um sistema de fosfato de antimônio contendo manganês. O objetivo geral desta pesquisa é sintetizar materiais inovadores que possuam atributos magneto-ópticos elevados e interessantes, com ênfase específica em seu potencial utilidade em dispositivos que aproveitem o efeito Faraday. O estudo apresenta diferentes experimentos para determinar as características térmicas, ópticas, luminescentes, estruturais, magnéticas e magneto-ópticas dos sistemas propostos, garantindo um conhecimento aprofundado de diferentes técnicas, conceitos e métodos, importantes para aumentar o crescimento científico em química e físico-química de materiais não-cristalinos. Foram obtidos excelentes valores de constante de Curie, até  $6.77 \text{ emu.Oe}^{-1}.\text{mol}^{-1}$ , valores maiores que relatados na literatura, e constante de Verdet de  $124 \text{ rad.T}^{-1}.\text{m}^{-1}$  a  $632.8 \text{ nm}$  para amostra com 27.5 %mol de  $\text{Tb}_2\text{O}_3$ , comparáveis a vidros e monocristais comerciais, e  $-55.1 \text{ rad.T}^{-1}.\text{m}^{-1}$  para a amostra 30%mol de  $\text{MnO}$ , valores inéditos para esse tipo de rotador Faraday. Ao examinar o impacto de composições variadas nas propriedades estruturais, ópticas e magnéticas dos materiais resultantes, esta tese contribui para uma compreensão mais profunda da interação entre metais de transição, terras raras e o comportamento magneto-óptico de vidros. Além disso, a tese avalia a capacidade dessas composições de vidro em exibir rotação de Faraday. Os insights obtidos com essa pesquisa não apenas avançam no conhecimento fundamental sobre a influência desses íons paramagnéticos na resposta magneto-óptica, mas também abrem caminho para o design e a realização de novos materiais magneto-ópticos. Como resultado de investigação rigorosa, esta tese de doutorado contribui significativamente para a compreensão científica e desenvolvimento prático de materiais preparados para moldar a perspectiva de aplicações magneto-ópticas.

---

## Résumé

L'étude et la préparation de nouveaux matériaux magnéto-optiques ont fait l'objet d'une attention particulière en raison de leurs applications potentielles dans divers domaines technologiques. Les verres qui supportent de fortes concentrations d'ions paramagnétiques sont largement recherchés à ces fins, en raison des propriétés inhérentes aux verres telles que l'isotropie, la fenêtre de transmission élevée, les indices de réfraction élevés, la synthèse et la modélisation faciles, toutes des propriétés intéressantes pour les systèmes optiques. Cette thèse de doctorat étudie le domaine de la science des matériaux avancés, en étudiant la synthèse et la caractérisation complète de deux systèmes vitreux, un borotungstate contenant d'abord du terbium et plus tard une étude étendue à d'autres lanthanides, et un système de phosphate d'antimoine contenant du manganèse. L'objectif global de cette recherche est de synthétiser des matériaux innovants qui ont des attributs magnéto-optiques élevés et intéressants, avec un accent particulier sur leur utilité potentielle dans les dispositifs qui tirent parti de l'effet Faraday. L'étude présente différentes expériences pour déterminer les caractéristiques thermiques, optiques, luminescentes, structurales, magnétiques et magnéto-optiques des systèmes proposés, garantissant une connaissance approfondie des différentes techniques, concepts et méthodes, importants pour accroître la croissance scientifique en chimie et physique chimique des matériaux non cristallins. D'excellentes valeurs de constante de Curie ont été obtenues, jusqu'à  $6,77 \text{ emu.Oe}^{-1}.\text{mol}^{-1}$ , valeurs supérieures à celles rapportées dans la littérature, et une constante de Verdet de  $124 \text{ rad.T}^{-1}.\text{m}^{-1}$  à  $632,8 \text{ nm}$  pour un échantillon de  $27,5 \text{ \% mol de Tb}_2\text{O}_3$ , comparable aux verres et monocristaux commerciaux, et  $-55,1 \text{ rad.T}^{-1}.\text{m}^{-1}$  pour l'échantillon à  $30\% \text{ mol MnO}$ , des valeurs sans précédent pour ce type de rotateur de Faraday. En examinant l'impact de différentes compositions sur les propriétés structurales, optiques et magnétiques des matériaux résultants, cette thèse contribue à une compréhension plus approfondie de l'interaction entre les métaux de transition, les terres rares et le comportement magnéto-optique des verres. De plus, la thèse évalue la capacité de ces compositions de verre à présenter une rotation de Faraday. Les connaissances acquises grâce à cette recherche font non seulement progresser les connaissances fondamentales sur l'influence de ces ions paramagnétiques sur la réponse magnéto-optique, mais ouvrent également la voie à la conception et à la réalisation de nouveaux matériaux magnéto-optiques. Fruit de recherches rigoureuses, cette thèse de doctorat contribue de manière significative à la compréhension scientifique et au développement pratique de matériaux prêts à façonner les perspectives d'applications magnéto-optiques.

---

## Abstract

The study and preparation of new magneto-optical materials has gained significant attention due to their potential applications in various technological domains. Glasses that support high concentrations of paramagnetic ions are being widely sought after for these purposes, due to the inherent properties of glasses such as isotropy, high transmission window, high refractive indexes, easy synthesis and modelling, all interesting properties for optical systems. This doctoral thesis investigates the domain of advanced materials science, investigating the synthesis and comprehensive characterization of two glassy systems, a borotungstate containing first terbium and later an extended study to other lanthanides, and an antimony phosphate system containing manganese. The overall objective of this research is to synthesize innovative materials that have high and interesting magneto-optical attributes, with specific emphasis on their potential utility in devices that take advantage of the Faraday effect. The study presents different experiments to determine the thermal, optical, luminescent, structural, magnetic and magneto-optical characteristics of the proposed systems, guaranteeing an in-depth knowledge of different techniques, concepts and methods, important to increase the scientific growth in chemistry and chemical physics of non-crystalline materials. Excellent Curie constant values were obtained, up to  $6.77 \text{ emu.Oe}^{-1}.\text{mol}^{-1}$ , values higher than those reported in the literature, and Verdet constant of  $124 \text{ rad.T}^{-1}.\text{m}^{-1}$  at  $632.8 \text{ nm}$  for a sample with 27.5% mol of  $\text{Tb}_2\text{O}_3$ , comparable to commercial glasses and single crystals, and  $-55.1 \text{ rad.T}^{-1}.\text{m}^{-1}$  for the 30% mol  $\text{MnO}$  sample, unprecedented values for this type of Faraday rotator. By examining the impact of varying compositions on the structural, optical, and magnetic properties of the resulting materials, this thesis contributes to a deeper understanding of the interplay between transition metals, rare earths, and the magneto-optical behavior of glasses. Furthermore, the thesis evaluates the ability of these glass compositions to exhibit Faraday rotation. The insights gained from this research not only advance fundamental knowledge about the influence of these paramagnetic ions on magneto-optical response, but also pave the way for the design and realization of new magneto-optical materials. As a result of rigorous research, this doctoral thesis contributes significantly to the scientific understanding and practical development of materials poised to shape the prospect of magneto-optical applications.

---

## List of Figures

- Figure 1.** The Lycurgus Cup in reflected (a) and transmitted (b) light. Scene showing Lycurgus being enmeshed by Ambrosia, now transformed into a vine-shoot [The Trustees of the British Museum, Department of Prehistory and Europe, The British Museum. Height: 16.5 cm (with modern metal mounts), diameter: 13.2 cm][13]. ..... 37
- Figure 2.** Two-dimensional schematic representation illustrating the difference between: (a) the symmetrical and periodic crystalline arrangement of a crystal of composition  $A_2O_3$ ; (b) representation of the glass network of the same compound, in which the absence of symmetry and periodicity is characterized. (Adapted from [31]) ..... 40
- Figure 3.** Atomic-resolution images of a 2D glass. (a,b) Zachariassen's models for a 2D crystal and a 2D amorphous glass. (c,d) Experimental TEM images of 2D crystalline and amorphous silica supported by graphene.[32]..... 41
- Figure 4.** The volume-temperature diagram for a glass-forming liquid. *abc* path is related to the transition from a liquid to a conventional solid, with the transformation taking place at the melting point. *ade* path corresponds to a decrease in temperature and increase in viscosity of the liquid, becoming a supercooled liquid, and finally, with a sudden decrease in temperature and increase in viscosity, forming a glass. *afg* path corresponds to the same transformation, but with faster quenching. (Adapted from [43]). ..... 46
- Figure 5.** Variation of molar susceptibility for each atom. For some, the diamagnetic effect is dominant, mainly due to the filling of the valence orbitals. Negative values indicate that they are repelled by the external magnetic field,  $B$ . For others, the paramagnetic effect is the most relevant, due to the number of half-filled orbitals. Positive values show that they are attracted by  $B$ . Fe, Co and Ni atoms have naturally high susceptibility, promoting ferromagnetic characteristics [Figure from Stan Zurek, Magnetic susceptibility, Encyclopedia Magnetica]. 50
- Figure 6.** (a) Paramagnetic (black) and diamagnetic (blue) susceptibility versus temperature under constant applied magnetic field. Inset of shown the inverse of paramagnetic susceptibility versus temperature, varying linearity. (b) Curie's law deviation, with three different Weiss temperatures,  $\theta < 0$ ,  $\theta = 0$  and  $\theta > 0$ . [Adapted from [47]]..... 53
- Figure 7.** The magnetic family tree, showing the evolution of macro-magnetic properties, the behavior of magnetic susceptibility, the organization of spins and some examples of substances that have these effects, making clear the complexity of magnetic effects[47]. ..... 55
- Figure 8.** Behavior of (a) magnetic susceptibility and (b) of the inverse magnetic susceptibility for paramagnetic (red), ferromagnetic (blue) and antiferromagnetic (green) substances with temperature variation, under constant external magnetic field, showing  $T_C$  and  $T_N$ . (c) Representation of spin alignment for ferromagnetic (parallel alignment), antiferromagnetic (antiparallel alignment) and ferrimagnetic (antiparallel alignment with differences in intensity A and B) substances. [Adapted from [47] ..... 57

---

<b>Figure 9.</b> Schematic figure of a Faraday rotator. Polarizer light $\lambda$ passes through the medium with optical path $l$ , under the external magnetic field and constant $B$ , causing a rotation of the plane of polarization of light, measured at angle $\beta$ . [Extracted from ThorLabs – Faraday Rotators page. <a href="https://www.thorlabs.com/images/TabImages/Faraday_Rotator_Diagram_D1-780.gif">https://www.thorlabs.com/images/TabImages/Faraday_Rotator_Diagram_D1-780.gif</a> ] .....	59
<b>Figure 10.</b> “ <i>Magneto-optical sensors</i> ” publications and citations made by Web of Science on April 14, 2023 [from Web of Science searching “ <i>Magneto-optical sensors</i> ”]. .....	64
<b>Figure 11.</b> “ <i>Magneto-optical glasses</i> ” publications and citations made by Web of Science on April 14, 2023 [from Web of Science searching “ <i>Magneto-optical glasses</i> ”]. .....	64
<b>Figure 12.</b> Magnetic signals produced by various sources[81]. .....	66
<b>Figure 13.</b> Dependence of $V$ on $Tb^{3+}$ ion concentration and comparison to other reported data glasses at a fixed wavelength of 632.8 nm [87]. .....	67
<b>Figure 14.</b> Ternary diagram of compositions in the $Tb_2O_3$ - $WO_3$ - $B_2O_3$ system. Green spheres correspond to glass samples and red square to crystallized compositions. The $xTb_2O_3$ -(60-x) $B_2O_3$ -40 $WO_3$ (in mol %) series was chosen to study in this work. (Own authorship). .....	85
<b>Figure 15.</b> Binary phase diagram for the system $WO_3$ - $B_2O_3$ . [Adapted from [1]] .....	86
<b>Figure 16.</b> Energy diagram representing the principle of Raman scattering compared to Rayleigh scattering, anti-Stokes scattering, and electronic and IR absorption. (Own authorship). .....	94
<b>Figure 17.</b> Experimental scheme for the refraction index measurement using the Brewster angle method. The graph on the side shows an example of the angular scan for the 25 $Tb$ 40 $W$ sample at 532 nm. The red fit represents the adjustment of the parameters allowing the index to be extracted in the used wavelength. (Adapted from[7]) .....	97
<b>Figure 18.</b> Scheme (a) and real apparatus (b) for Faraday effect measurements. Light from the 632.8 nm laser passes through the polarizer, then through the sample under the $B$ field, which causes a rotation on the axis of polarization of the light. This deflection is measured on the second polarizer. (Own authorship).....	99
<b>Figure 19.</b> Samples $xTb_2O_3$ -(60-x) $B_2O_3$ -40 $WO_3$ series, after cut and polishing, with their specific names. (Own authorship). .....	103
<b>Figure 20.</b> $xTb$ 40 $W$ samples diffractograms and $YBO_3$ analogous phase. (Own authorship). .....	105
<b>Figure 21.</b> DSC curves (a), $T_g$ and $\Delta T$ variation (b) for $xTb$ 40 $W$ samples. (Own authorship). .....	106

---

<b>Figure 22.</b> Theoretical optical basicity ( $\Lambda_{th}$ ) and density ( $\rho$ ) for the samples varying the $Tb^{3+}$ ion effective concentration. (Own authorship).....	108
<b>Figure 23.</b> Raman scattering spectroscopy for the samples with different concentrations of $Tb_2O_3$ , in addition to 25La40W sample, mimicking the 25Tb40W sample. (Own authorship). .....	110
<b>Figure 24.</b> $^{11}B$ MAS-NMR for the sample 25La40W, mimetizing sample 25Tb40W. (Own authorship).....	112
<b>Figure 25.</b> Normalized infrared absorption spectra, obtained by DRIFT, for xTb40W samples and 25La40W. (Own authorship). ....	113
<b>Figure 26.</b> Absorption coefficient spectra of the xTb40W samples, with the respective absorption band. (Own authorship). ....	114
<b>Figure 27.</b> Transmittance spectra of the terbium-containing samples, with the respective absorption bands. (Own authorship).....	115
<b>Figure 29.</b> Refractive index for samples with different contents of $Tb_2O_3$ in the ternary system and Cauchy's Law for the witch sample. (Own authorship).....	116
<b>Figure 29.</b> Normalized excitation spectra for the samples with different concentrations of $Tb_2O_3$ , showing the 4f-4f transitions ( $^7F_6 \rightarrow$ ) under $\lambda_{em} = 543$ nm. (Own authorship).....	118
<b>Figure 30.</b> Emission spectra for xTb40W samples, showing the 4f- 4f ( $^5D_4$ and $^5D_3 \rightarrow$ ) transitions under $\lambda_{exc} = 379$ nm. ....	119
<b>Figure 31. a.</b> CIE 1931 chromaticity diagram for xTb40W samples under 379 nm excitation. <b>b.</b> Partial energy level diagram of $Tb^{3+}$ illustrating the excitation $^7F_6 \rightarrow ^5D_3 + ^5G_6$ , non-radiative decay (NR; $^5D_3 \rightarrow ^5D_4$ ), emissions $^5D_4 \rightarrow ^7F_J$ , and cross-relaxation process (CR) between two neighboring $Tb^{3+}$ ions.....	120
<b>Figure 32.</b> Measured magnetic susceptibility for the 25Tb40W sample, measured by zero field-cooled (ZFC) and field-cooled (FC) methods. (Own authorship).....	121
<b>Figure 33.</b> Temperature dependence of the paramagnetic molar susceptibility for all samples. Inset shown the inverse of susceptibility ( $1/\chi_{para}$ ) versus temperature, varying linearity and follow the Curie-Weiss law. (Own authorship).....	122
<b>Figure 34.</b> Variation of the Verdet constant by concentration of $Tb^{3+}$ ions for the samples (red squares), some reference crystals (black stars) and different glass families (spheres): aluminosilicates (black), borates (red), borogermanates (orange), borogermanosilicates (yellow), borosilicates (green), fluorides (turquoise), fluorophosphates (blue) and phosphates glasses (purple). The dash line represent a fit of the data. (Own authorship). ....	125

---

<b>Figure 35.</b> Behavior of the Verdet constant of the xTb40W samples (red squares) compared with commercially used crystals (black stars). (Own authorship). .....	126
<b>Figure 37.</b> Samples for the 25Ln <sub>2</sub> O <sub>3</sub> -35B <sub>2</sub> O <sub>3</sub> -40WO <sub>3</sub> system, where a. Ln = Sm, Eu, Gd, Dy, Ho, and a sample with 12.5Tb <sub>2</sub> O <sub>3</sub> -12.5Gd <sub>2</sub> O <sub>3</sub> -35B <sub>2</sub> O <sub>3</sub> -40WO <sub>3</sub> and b. Ln = Er, Nd, Tm. (Own authorship). .....	138
<b>Figure 38.</b> Photo sequence of the 25Ho40W sample being attracted by a neodymium magnet at room temperature. The high concentration of paramagnetic species imparts this effect to the samples. (Own authorship). .....	140
<b>Figure 39.</b> X-ray diffractograms for the 25Ln40W, Ln = Nd, Sm, Eu, Gd, Tb, Dy, Ho, Er or Tm samples, the ionic radius for the respective Ln <sup>3+</sup> ion and the TmBO <sub>3</sub> standard, hexagonal phase group P63/mmc (CIF-1511089). (Own authorship). .....	141
<b>Figure 40.</b> DSC curves for the 25Ln40W samples. (Own authorship). .....	142
<b>Figure 41.</b> T <sub>g</sub> and ΔT variation for each lanthanide ionic radius of 25Ln40W samples. (Own authorship). .....	144
<b>Figure 42.</b> a) Variation of effective ionic concentration and b) theoretical optical basicity and density for 25Ln40W samples, compared by different ionic radii of Ln <sup>3+</sup> . For the 12.5TbGd40W sample, the averages of the Tb <sup>3+</sup> and Gd <sup>3+</sup> radii were considered, as they represent half the concentration of each. (Own authorship). .....	145
<b>Figure 43.</b> Raman spectra for each 25Ln40W sample. (Own authorship). .....	146
<b>Figure 44.</b> Normalized absorption coefficient for each sample 25Ln40W obtained Kramers-Kronig transform from infrared measurement by specular reflectance. The inset graph shows the absolute values for each sample. (Own authorship). .....	148
<b>Figure 45.</b> Transparency window for the 25Sm40W sample, with its main assignments starting from the ground state <sup>6</sup> H <sub>5/2</sub> . (Own authorship). .....	149
<b>Figure 46.</b> Zoom 0.2-0.8 μm transmittance spectra for the 25Sm40W sample, with its main assignments starting from the ground state <sup>6</sup> H <sub>5/2</sub> . (Own authorship). .....	150
<b>Figure 47.</b> Zoom 0.8-1.75 μm transmittance spectra for the 25Sm40W sample, with its main assignments starting from the ground state <sup>6</sup> H <sub>5/2</sub> . (Own authorship). .....	150
<b>Figure 48.</b> Transparency window for the 25Eu40W sample, with its main assignments starting from the ground state <sup>7</sup> F <sub>0</sub> . (Own authorship). .....	151
<b>Figure 49.</b> Transparency window for the 25Gd40W sample, with its main assignments starting from the ground state <sup>8</sup> S <sub>7/2</sub> . (Own authorship). .....	152

---

<b>Figure 50.</b> Transparency window for the 12.5TbGd40W sample, with its main assignments starting from the ground state $^7F_6$ . 25Tb40W sample was taken as a reference. (Own authorship).....	153
<b>Figure 51.</b> Transparency window for the 25Dy40W sample, with its main assignments starting from the ground state $^6H_{15/2}$ . (Own authorship).....	154
<b>Figure 52.</b> Zoom 0.2-0.7 $\mu\text{m}$ transmittance spectra for the 25Dy40W sample, with its main assignments starting from the ground state $^6H_{15/2}$ . (Own authorship).....	154
<b>Figure 53.</b> Zoom 0.7-1.6 $\mu\text{m}$ transmittance spectra for the 25Dy40W sample, with its main assignments starting from the ground state $^6H_{15/2}$ . (Own authorship).....	155
<b>Figure 54.</b> Transparency window for the 25Ho40W sample, with its main assignments starting from the ground state $^5I_8$ . (Own authorship).....	156
<b>Figure 55.</b> Zoom 0.2-85 $\mu\text{m}$ transmittance spectra for the 25Ho40W sample, with its main assignments starting from the ground state $^5I_8$ . (Own authorship).....	156
<b>Figure 56.</b> PL spectra for the Sm40W sample, showing the transitions from the excited level $^4G_{5/2}$ corresponding to the $\text{Sm}^{3+}$ ion. $\lambda_{\text{exc}} = 404 \text{ nm}$ . (Own authorship).....	157
<b>Figure 57.</b> PL spectra for Eu40W sample, with the 4f-4f transitions from the excited level $^5D_0$ , corresponding to the $\text{Eu}^{3+}$ ion. $\lambda_{\text{exc}} = 394 \text{ nm}$ . (Own authorship).....	158
<b>Figure 58.</b> PL spectra for the 12.5TbGd40W sample, showing the transitions from the excited level $^5D_4$ corresponding to the $\text{Tb}^{3+}$ ion. $\lambda_{\text{exc}} = 379 \text{ nm}$ . (Own authorship).....	159
<b>Figure 59.</b> PL spectra for the 25Dy40W sample, showing the transitions from the excited level $^5F_{9/2}$ corresponding to the $\text{Dy}^{3+}$ ion. $\lambda_{\text{exc}} = 352 \text{ nm}$ . (Own authorship). ....	160
<b>Figure 60.</b> PL spectra for the 25Ho40W sample, showing the transitions corresponding to the $\text{Ho}^{3+}$ ion. $\lambda_{\text{exc}} = 455 \text{ nm}$ . (Own authorship). ....	161
<b>Figure 61.</b> Partial energy level diagram of samples $\text{Ln}^{3+}$ ions and the radiative transitions emissions [[29]]. .....	162
<b>Figure 62.</b> Refractive index for Ln trivalent ions glass samples. (Own authorship). .....	163
<b>Figure 63.</b> Temperature dependence of the paramagnetic molar susceptibility for all 25Ln40W glass samples. Inset shown the inverse of susceptibility ( $1/\chi_{\text{para}}$ ) versus temperature, varying linearity and follow the Curie-Weiss law. (Own authorship).....	165
<b>Figure 64.</b> Inverse of susceptibility by temperature for the samples 25Sm40W and 25Eu40W. ....	166

---

<b>Figure 65.</b> Photography of the glasses containing MnO studied in this work. (Own authorship). .....	171
<b>Figure 66.</b> Sequence of photographs showing the attractive response of the glasses to the presence of a Nd-based magnet. a) and b) represent the approximation of the magnet, while the sequence after is related to the suspension of the glass piece (from c to f). (Own authorship). .....	172
<b>Figure 67.</b> X-ray diffraction data for SZPxMn samples. ....	173
<b>Figure 68.</b> DSC curves for each SZPxMn sample, with arrow indicating the variation of T <sub>g</sub> and T <sub>x</sub> . (Own authorship). ....	174
<b>Figure 69.</b> Raman scattering spectra of the samples SZPxMn with the main assignments. (Own authorship). ....	175
<b>Figure 70.</b> Infrared spectrum for each sample of the SZPxMn system, with the main bands marked. (Own authorship). ....	176
<b>Figure 71.</b> Molar volume (V <sub>M</sub> ) and density (ρ) variation for ion effective concentration (N <sub>Mn<sup>2+</sup></sub> ) of which SZPxMn series samples. (Own authorship). ....	178
<b>Figure 72.</b> (a) Transmittance windows and (b) absorption coefficient spectra in SZPxMn system, with the mains transitions (Mn <sup>2+</sup> in black and Mn <sup>3+</sup> in blue) assigned. (Own authorship). .....	180
<b>Figure 73.</b> Excitation (a), with λ <sub>em</sub> = 720 nm, and emission (b), with λ <sub>exc</sub> = 410 nm, spectra for samples SZPxMn system. (Own authorship). ....	181
<b>Figure 74.</b> (a) Zero-field-cooled (ZFC) and field-cooled (FC) susceptibility (χ <sub>DC</sub> ) as a function of the temperature (T) for the 1-x(SbPO <sub>4</sub> -ZnO-PbO)-xMnO glass with an applied magnetic field of H = 100 Oe. (b) χ <sub>DC</sub> - 1 vs T curve for the 30, 20, and 10 MnO containing, where the point represents the experimental data and the blue dashed line represents the fits to the Curie-Weiss law (Eq. 28). (c) Magnetization as a function of the applied magnetic field (M vs. H) loops at 5K (d) and 300 (K). The yellow continue line represents the Brillouin function fit. (Own authorship). ....	182
<b>Figure 75.</b> μ <sub>eff</sub> obtained from the analyses, where also the obtained values using Curie-Weiss law were included for comparison. (Own authorship). ....	185
<b>Figure 76.</b> Verdet constant (V) versus effective Mn <sup>2+</sup> concentration (N <sub>Mn<sup>2+</sup></sub> ) for SZPxMn series samples. (Own authorship). ....	186

---

## List of Figures in Appendix

- Figure A-1.** Photograph of the 3D inscription attempts performed on the 25Tb40W sample, taken with a 40X objective lens. For high powers(A-1a), the formation of holes occurred and for low powers (A-1b), weak and discontinuous markings occurred..... 195
- Figure A-2.** Preforms after trying to draw the fibers. A crystalline phase is observed in the region where preform heating occurred..... 196
- Figure A-3.** Schematic illustration of the coupling between the Faraday effect (FE) and the inverse Faraday effect (IFE) in a liquid [7]. ..... 198

---

## List of Tables

<b>Table 1.</b> Theoretical values of $\chi_{\text{dia}}$ for some ions[56].....	51
<b>Table 2.</b> Series of Tb-contain borotungstate glasses, showing name, nominal compositions (in mol % and cat mol %), molar mass (M) and if phase separation occurred during quenching. ....	103
<b>Table 3.</b> Thermal and physical properties of the glass samples: Tg (glass transition temperature), Tx (onset of the crystallization temperature), $\Delta T$ (thermal stability parameter), $\rho$ (density), NTb <sup>3+</sup> (ion effective concentration), $\Lambda_{\text{Th}}$ (theoretical optical basicity) and $\lambda_{\text{UV}}$ (short wavelength cut-off). ....	106
<b>Table 4.</b> Band assignments of the main vibrational modes in Raman for the xTb40W glasses. ....	110
<b>Table 5.</b> Refractive indices for xTb40W samples, at wavelengths 532, 639, 785, 935 nm with $\pm 0.005$ error. We obtained the refractive index for 1000 nm using Cauchy's Law.....	117
<b>Table 6.</b> theoretical diamagnetic susceptibility ( $\chi_{\text{dia}}$ ), Weiss temperature ( $\theta$ ), Curie constant (C) for two units (one in Oested, Oe, e other in Tesla, T) and probed Tb <sub>2</sub> O <sub>3</sub> % mol for each sample. ....	122
<b>Table 7.</b> comparison between different Curie constant (C) values and Weiss temperature ( $\theta$ ) for samples from this work and examples from the literature. ....	123
<b>Table 8.</b> Series of Ln-contain borotungstate glasses, showing name, nominal compositions (% mol and % cat mol), molar mass (M) and if phase separation occurred during quenching. ..	139
<b>Table 9.</b> Thermal and physical properties of the glass samples: Tg (glass transition temperature), Tx (onset of the crystallization temperature), $\Delta T$ (thermal stability parameter), $\rho$ (density), NLn <sup>3+</sup> (ion effective concentration), $\Lambda_{\text{Th}}$ (theoretical optical basicity) and $\lambda_{\text{UV}}$ (short wavelength cut-off). ....	142
<b>Table 10.</b> Band assignments of the main vibrational modes in Raman and Infrared for the 25Ln40W glasses.....	147
<b>Table 11.</b> Refractive index values for samples with different trivalent lanthanide ions for different laser wavelengths (error = $\pm 0.005$ ). ....	163
<b>Table 12.</b> Fundamental level of Ln <sup>3+</sup> , spin angular momentum (S), orbital angular momentum (L), total angular momentum (J), diamagnetic susceptibility ( $\chi_{\text{dia}}$ ), Weiss temperature ( $\theta$ ), Curie constant (C) in two different units and Ln <sub>2</sub> O <sub>3</sub> % mol for each 25Ln40W samples. ...	165

---

<b>Table 13.</b> Chemical compositions and characteristic temperatures of the glasses studied in this work. The thermal stability parameter ( $\Delta T$ ) and the refractive index ( $\lambda_{\text{laser}} = 532 \text{ nm}$ ) of the samples are also shown. ....	171
<b>Table 14.</b> Raman scattering and infrared band assignments for SZP $\times$ Mn series.....	176
<b>Table 15.</b> Density ( $\rho$ ), ion effective concentration (NMn $^{2+}$ ), theoretical optical basicity ( $\Delta Th$ ), short wavelength cut-off ( $\lambda_{UV}$ ) and refractive index ( $n$ ) at 532 nm for samples SZP $\times$ Mn...	177
<b>Table 16.</b> Parameters obtained from the fits of the susceptibility ( $\chi_{DC}$ ) versus temperature ( $T$ ) to the Curie–Weiss law as described in the text. ....	183

---

## List of Equations

Gauss's law.....	(Eq. 1)
Gauss' s law for magnetism.....	(Eq.2)
Faraday' s law of induction.....	(Eq.3)
Ampère' s circuital law.....	(Eq.4)
Magnetic suscetibility.....	(Eq. 5)
Diamagnetic susceptibility.....	(Eq. 6)
Spin (S), orbital (L), and total angular momentum (J).....	(Eq. 7)
Curie's law.....	(Eq.8)
Curie constant.....	(Eq.9)
Landé g-factor.....	(Eq.10)
Curie–Weiss law.....	(Eq.11)
Faraday effect.....	(Eq.12)
Verdet constant, diamagnetic contribution.....	(Eq.13)
Verdet constant, paramagnetic contribution.....	(Eq.14)
Verdet constant, paramagnetic contribution correction.....	(Eq.15)
Relationship between V and $\alpha$ .....	(Eq.16)
Archimedes' principle.....	(Eq.17)
Kramers-Krönig inversion technique.....	(Eq.18-23)
Ion effective concentration.....	(Eq.24)
Theoretical optical basicity.....	(Eq.25)
Figure of merit.....	(Eq.26)
Curie-Weiss Law for Mn.....	(Eq.27)
Inverse of Eq.27.....	(Eq.28)
Magnetization x Field.....	(Eq.29)
Magnetization x Field simplified.....	(Eq.30)

---

## Summary

<b>CHAPTER I - INTRODUCTION</b>	<b>35</b>
<b>1. GLASSES</b>	<b>35</b>
1.1. BRIEF HISTORY OF THE EMERGENCE OF GLASSWORKING, GLASSMAKING AND PHOTONIC GLASSES.	35
1.2. DEVELOPMENT OF THE DEFINITION OF GLASSES.	39
1.3. GLASS FORMATION FROM A MELT.	45
<b>2. MAGNETO-OPTICAL PROPERTIES</b>	<b>46</b>
2.1 BRIEF HISTORY OF MAGNETISM AND MAGNETO-OPTICAL EFFECT.	46
2.2. MAGNETISM IN ATOMS AND MACROSCOPIC MAGNETIC PROPERTIES OF MATERIALS.	48
2.3 PRINCIPLES OF THE MAGNETO-OPTICAL FARADAY EFFECT.	59
2.4 STATE OF THE ART OF FARADAY ROTATOR GLASSES.	63
<b>REFERENCES IN THIS CHAPTER</b>	<b>71</b>
<b>OBJECTIVES OF THIS WORK</b>	<b>82</b>
<b>CHAPTER II – EXPERIMENTAL TECHNIQUES</b>	<b>84</b>
<b>1. SYNTHESIS OF THE SAMPLES</b>	<b>84</b>
1.1. $Tb_2O_3$ - $B_2O_3$ - $WO_3$ SYSTEM	84
1.2. $Ln_2O_3$ - $B_2O_3$ - $WO_3$ SYSTEM	86
1.3. $SbPO_4$ SYNTHESIS	87
1.4. $SbPO_4$ - $ZNO$ - $PBO$ - $MNO$ SYSTEM	88
<b>2. INSTRUMENTAL METHODS</b>	<b>88</b>
2.1. THERMAL ANALYSIS	88
2.2. X-RAY DIFFRACTOMETRY	89
2.3. DENSITY MEASUREMENTS	90
2.4. FOURIER-TRANSFORM INFRARED SPECTROSCOPY	91
2.5. RAMAN SCATTERING SPECTROSCOPY	93
2.6. $^{11}B$ -NUCLEAR MAGNETIC RESONANCE	95
2.7. UV-VISIBLE-NIR SPECTROSCOPY	95
2.8. REFRACTIVE INDEX MEASUREMENTS	96
2.9. FLUORESCENCE SPECTROSCOPY	97
2.10. MAGNETIC SUSCEPTIBILITY MEASUREMENTS	98
2.11. FARADAY EFFECT MEASUREMENTS	99
<b>REFERENCES IN THIS CHAPTER</b>	<b>101</b>
<b>CHAPTER III - CHARACTERIZATION AND STUDY OF PROPERTIES OF THE <math>Tb_2O_3</math>-<math>B_2O_3</math>-<math>WO_3</math> SYSTEM</b>	<b>103</b>
<b>1. SAMPLES</b>	<b>103</b>
<b>2. XRD.</b>	<b>104</b>
<b>3. THERMAL ANALYSIS</b>	<b>105</b>
<b>4. DENSITY AND OPTICAL BASICITY</b>	<b>106</b>
<b>5. STRUCTURAL ANALYSIS</b>	<b>109</b>
<b>6. UV-VIS-NIR SPECTROSCOPIES.</b>	<b>113</b>

7. REFRACTIVE INDEX.	116
8. FLUORESCENCE SPECTROSCOPY.	117
9. MAGNETIC SUSCEPTIBILITY	120
10. MAGNETO-OPTICAL MEASUREMENTS	124
11. PARTIAL CONCLUSIONS OF THIS CHAPTER.	126
REFERENCES IN THIS CHAPTER	128

#### **CHAPTER IV - CHARACTERIZATION AND STUDY OF PROPERTIES OF THE $\text{LN}_2\text{O}_3\text{-B}_2\text{O}_3\text{-WO}_3$ SYSTEM** 137

1. SAMPLES	137
2. XRD	140
3. THERMAL ANALYSIS AND DENSITY	142
4. DENSITY AND OPTICAL BASICITY	144
5. STRUCTURAL ANALYSIS	145
6. OPTICAL ANALYSIS	149
7. LUMINESCENCE ANALYSIS	157
8. REFRACTIVE INDEX.	162
9. MAGNETIC ANALYSIS	163
10. PARTIAL CONCLUSIONS OF THIS CHAPTER.	166
REFERENCES IN THIS CHAPTER	167

#### **CHAPTER V - STUDY OF THE STRUCTURAL AND MAGNETIC PROPERTIES OF THE $\text{SBPO}_4\text{-ZNO-PBO-MNO}$ SYSTEM** 171

1. SAMPLES	171
2. XRD	173
3. THERMAL ANALYSIS	173
4. RAMAN SCATTERING AND INFRARED SPECTROSCOPY	175
5. DENSITY.	177
6. OPTICAL ANALYSIS	179
7. LUMINESCENCE ANALYSIS	180
8. MAGNETIC ANALYSIS	181
9. MAGNETO-OPTICAL ANALYSIS.	185
10. PARTIAL CONCLUSIONS OF THIS CHAPTER.	187
REFERENCES OF THIS CHAPTER.	188

#### **CHAPTER VI – FINAL CONCLUSION AND PERSPECTIVES** 192

#### **APPENDIX I – OTHER MEASUREMENTS AND EXPERIMENTS CARRIED OUT** 194

A-I. PHOTOCROMISM TESTS.	194
A-II. 3D INSCRIPTION.	194
A-III. OPTICAL FIBER DRAWING.	195
A-IV. MELTING-QUENCHING UNDER EXTERNAL MAGNETIC FIELD.	196
A-V. INVERSE FARADAY EFFECT MEASURES.	197
A-VI. MAGNETIC PROPERTIES UNDER IRRADIATION AT LOW TEMPERATURE.	198

---

REFERENCES IN THIS APPENDIX 199

**APPENDIX II – PERIODIC TABLE OF ELEMENTS 201**

**APPENDIX III – CARNALL DIAGRAM 202**

**APPENDIX IV – ACADEMIC TREE – LEONARDO VIEIRA ALBINO 203**

## CHAPTER I – Introduction



**Sixth Solvay Conference**, whose theme was "*Le magnétisme*". Paris, 1930 [47].

*Seated in front:* Th. de Donder, P. Zeeman, P. Weiss, A. Sommerfeld, M. Curie, P. Langevin, A. Einstein, O. Richardson, B. Cabrera, N. Bohr, W. J. De Haas;

*Standing:* E. Herzen, E. Henriot, J. Verschaffelt, C. Manneback, A. Cotton, J. Errera, O. Stern, A. Piccard, W. Gerlach, C. Darwin, P. A. M. Dirac, H. Bauer, P. Kapitsa, L. Brillouin, H. A. Kramers, P. Debye, W. Pauli, J. Dorfman, J. H. Van Vleck, E. Fermi, W. Heisenberg.

## Chapter I - Introduction

### **1. GLASSES**

#### **1.1. Brief history of the emergence of glassworking, glassmaking and photonic glasses.**

Looking at vitreous materials, from the most common and trivial to the most technological niche, it's difficult to grasp the antiquity of the crafting and production of this category of materials. Glass is one of the oldest materials to have been processed by mankind. As natural materials, found in the environment, and due to their characteristics of easy handling, being able to form excellent sharp flakes for making knives, arrowheads and spears, natural glasses, especially obsidian, were used by hominids for making tools from at least 500,000 years ago, during the Lower Paleolithic, in what is now Kenya [1].

Our species, *Homo sapiens*, did not appear until 315,000 years ago, so the art of manipulating glass predates humanity. With the expansion of *Homo sapiens* and the exit from Africa to Eurasia (90,000 years ago), and the discovery of new sites containing obsidian, this material continued to be used. During the Mesolithic (20,000 - 12,000 years ago) and Neolithic (12,000 - 7,500 years ago) periods, obsidian became increasingly important due to its ability to form more complex tools, including finer and sharper points, needles, hooks, knives, implements, jewelry, and various other items[2–6].

Artificial glass, on the other hand, is a relatively modern development, though still surprisingly old. Archaeological evidence suggests that non-crystalline, glass-like materials called faience were used in ancient Egypt, Mesopotamia, and Syria well before the production of glass itself [7]. Egypt's favorable preservation environment means that most of the early, well-studied glassware is located there, although some may have been imported[8,9]. The earliest known glass objects, which were beads dating back 5500 years ago, were likely produced by accident during metal smelting or by the production of faience, a vitrified ceramic formed by mixing crystalline and non-crystalline phases, using a high-temperature firing process. Significantly, the emergence

of high-temperature furnaces capable of melting copper and bronze allowed for the production of faience.[10]

Around 2600 BC, there is evidence of the first human-made glass, which was still quite opaque due to the technology of the time. Glass preparation techniques spread and improved with the expansion of the Bronze Age and trade between Asia Minor, Africa and Europe. As a result, increasingly complex pieces were produced, which were cheaper, more transparent, and had better results, such as in terms of shape and color.[11,12]

Jumping ahead to the Roman domain of the Mediterranean, it was the Romans who became the first people to dominate the making of transparent glass. They perfected the blowing method, which involves using a metallic pipe and leaving the molten material forming a bubble while shaping it. Additionally, the Romans excelled in the production of stained glass. They were also the pioneers of the technique of producing colored stained glass for churches by adding salts during synthesis, which was highly explored in the Middle Ages to create glass of different colors. Furthermore, we must acknowledge the Lycurgus cup depicted in Figure 1 that exhibits a unique attribute of having two colors, one when viewed from the outside (reflection) and the other when viewed from the inside (transmission). Researchers were highly intrigued until a more in-depth evaluation using transmission electron microscopy revealed the presence of gold and silver nanoparticles in glass, in specific sizes and shapes. This was one of the initial demonstrations of control over crystal growth and nanotechnology. The Lycurgus cup, dating back to the 4th century, remains an enigma regarding the process used by the ancient Romans to manufacture it [13].

The glasswork produced by guilds in Venice and on the Murano islands was a notable attraction for the city-state in the Middle Ages. The addition of lead in the glass melting process alongside the development of high-temperature furnaces produced transparent glasses with a higher refractive index. This advance gave rise to the lenses in early modern telescopes and microscopes. From the 16th century onwards, handmade glass in Bavaria became famous for dominating these properties. The production was a state secret for the Bavarians. Michael Faraday was interested in synthesizing these

glasses (lead borosilicates) at the beginning of his career at the Royal Institution in London. We will discuss this in the next sections.



**Figure 1.** The Lycurgus Cup in reflected (a) and transmitted (b) light. Scene showing Lycurgus being enmeshed by Ambrosia, now transformed into a vine-shoot [The Trustees of the British Museum, Department of Prehistory and Europe, The British Museum. Height: 16.5 cm (with modern metal mounts), diameter: 13.2 cm][13].

The glass industry was a part of the Industrial Revolution. Synthetic and refined raw materials were used for the first time in the production of windows and inert packaging. However, the unpredictability and non-homogeneity on an industrial scale were still problematic. The high, consistently accurate and reproducible optical qualities in glasses resulted from the joint efforts of Otto Schott, Carl Zeiss, and Ernst Abbe. They founded one of the pioneer glass companies, Glastechnische Laboratorium Schott & Genossen (current Schott & Associates Glass Technology Laboratory) based in Jena, capitalizing on their specialized skills. There have been significant advancements in developing new glass materials since then. For instance, the discovery of lanthanum-doped glasses in the 1930s [14], the development of no oxygen-containing chalcogenide

glasses in the 1953[15], with high transparency in the near and mid-infrared (NIR and MIR), the first metallic glass in 1960[16], the first glass laser in 1961[17], and the discovery of fluoride glasses in 1974 by Jacques Lucas, Michel and Marcel Poulain[18].

One of the most pertinent studies conducted on photonic glasses was the report by Charles K. Kao published in 1966 which concluded that the primary issue concerning the production of optical fibers for telecommunication was inadequate material purity. He predicted that fibers created from highly pure materials would exhibit a loss lower than 0.3 dB/km[19]. Consequently, Kao's accomplishment earned him the Nobel Prize in Physics in 2009. By 1970, fiber optics degradation of as low as 20 dB/km at 632.8 nm had already been achieved by Corning. In 1979, the preform and fiber production processes were further refined, decreasing the value to 0.20 dB/km at 1550 nm. Currently, the minimum attenuation in mass-produced single-mode fiber is less than 0.17 dB/km[20]. Optical fibers enabled and still enable information and knowledge to travel across the planet at the speed of light, they are the backbone of the Internet and the key to today's global communications revolution. During the COVID-19 pandemic, we made extensive use of long-distance conferencing services powered by fiber optics, which kept us together during those difficult times.

Glasses are present from the windows to cell phone screens. From beverage bottles to vaccine flasks. Composites made from bioglass have improved health care through their ability to integrate with human bone. Glass panels support solar cells and provide clean energy. The development of glass optics and optoelectronics means the James Webb Space Telescope can study the first moments after the Big Bang and expand our understanding of the universe. Glass artists around the world have introduced humanity to this wonderful material, including its remarkable fabrication methods, its inherent beauty, and its ability to capture and display nature's full spectrum of colors[21,22].

For these and many other reasons, the UN General Council declared 2022 as the International Year of Glass. Throughout history, we define ages by the materials and movements that transformed civilization, such as the Stone Age, Bronze Age, Iron Age, which provided revolutions in the civilizations that experienced them. And, as well proposed by David L. Morse and Jeffrey W. Evenson, both researchers at Corning

Incorporated, we currently live in the “Age of Glass”, due to all the social, cultural, and technological transformations associated with this class of material [23]. Welcome to the Glass Age!

## 1.2. Development of the definition of glasses.

Although glass has been used by humans for a long time, its definition has been the subject of several debates among scholars throughout history. One of the early pioneers in the study of glasses was the renowned physicist and chemist Michael Faraday (1791-1867), who defined them as follows:

“Glass may be considered rather as a solution of different substances one in another, than as a strong chemical compound.” Michael Faraday, 1830[24]

In the late 19th and early 20th centuries, Gustav Tammann (1861-1938) conducted experiments that proved the possibility of creating glasses from substances besides silica. To achieve ideal and homogeneous vitrification, it was essential to prevent the creation of crystalline nuclei, which leads to the expansion of macroscopic crystals. The possible vitrification process depends on the melting temperature of the material, the temperature for liquidus pouring, and/or tempering (a heat treatment used after glass formation to reduce post-quenching stress)[25]. After conducting these studies, glass definitions were formulated based on the viscosity of solids concept. This approach was necessary because, until then, glasses had only been prepared via the melting-quenching method, which involves rapidly cooling a molten substance. The viscosity criterion defines a solid as rigid material that doesn't flow when exposed to moderate forces. As a quantitative measure, a solid can be defined as a substance with a viscosity exceeding  $10^{14}$  Pa.s.

“Glass is non-crystalline, strongly supercooled melt inorganic product, which reaches a rigid condition by cooling, through a progressive increase in viscosity, without crystallization occurring.” Gustav Tammann, 1925[26]

The emergence of techniques such as X-ray diffraction and the initial results from measuring glass samples[27–30] revealed that the structural organization of glasses resembles that of liquids more than crystalline solids. In 1932, William Houlter Zachariasen, a Norwegian-American researcher, published the well-known article *'The Atomic Arrangement in Glass'*, where he formulated his Random Network Theory (RNT) in glasses while studying their diffractograms. Zachariasen established the structural basis for the formation of glasses by melting-quenching and suggested that “*the atomic arrangement in glasses was characterized by an extended three-dimensional network, which lacked symmetry and periodicity*”, and that “*interatomic forces were comparable to those of the corresponding crystal*”. Additionally, the researcher notes that the presence or absence of periodicity and symmetry in a three-dimensional network distinguishes between a crystal and a glass.[31]

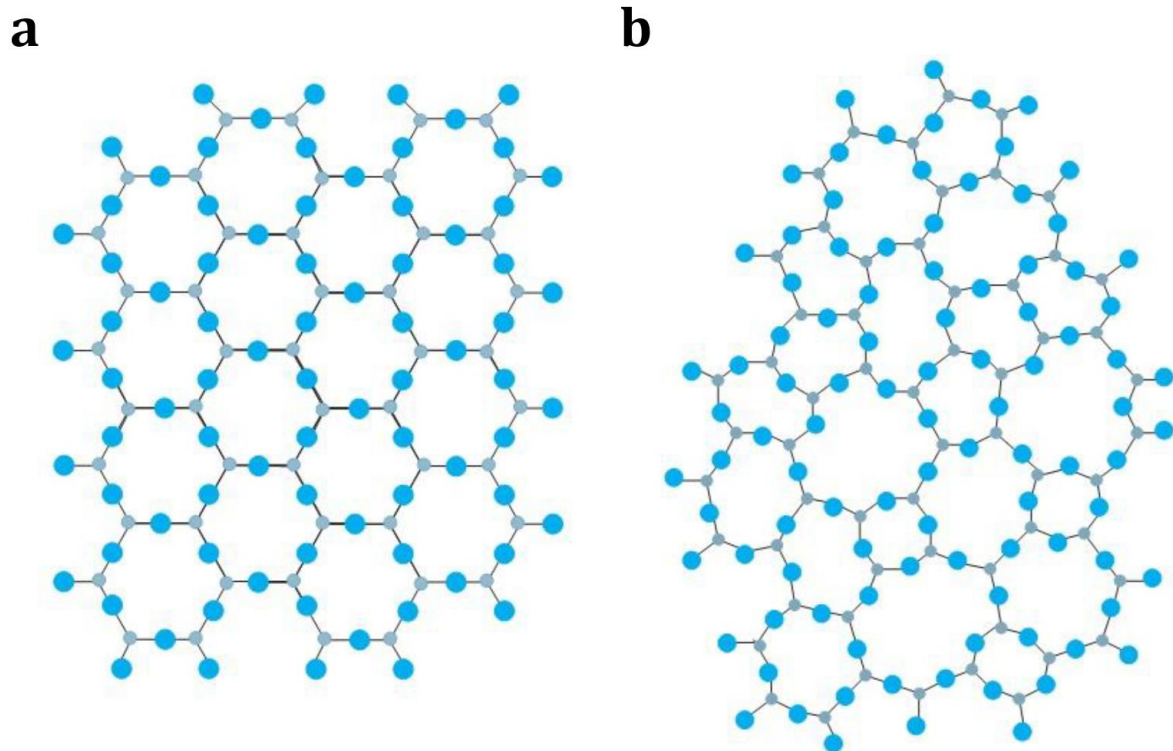


**Figure 2.** Two-dimensional schematic representation illustrating the difference between: (a) the symmetrical and periodic crystalline arrangement of a crystal of composition  $A_2O_3$ ; (b) representation of the glass network of the same compound, in which the absence of symmetry and periodicity is characterized. (Adapted from [31])

Figure 2a shows the symmetric and periodic crystal arrangement of a crystal composition  $A_2O_3$  in a two-dimensional format, while Figure 2b shows the glass network for the same compound, demonstrating the absence of symmetry and periodicity. This theory made the article a landmark in Glass Science. By combining Zachariasen's RNT and the contemporary concept of glass at the time of publication, we may arrive at the following definition:

“Glasses are described as supercooled liquids or as solids, with absence of periodicity in the network, isotropic materials.”

William H. Zachariasen, 1932[31]

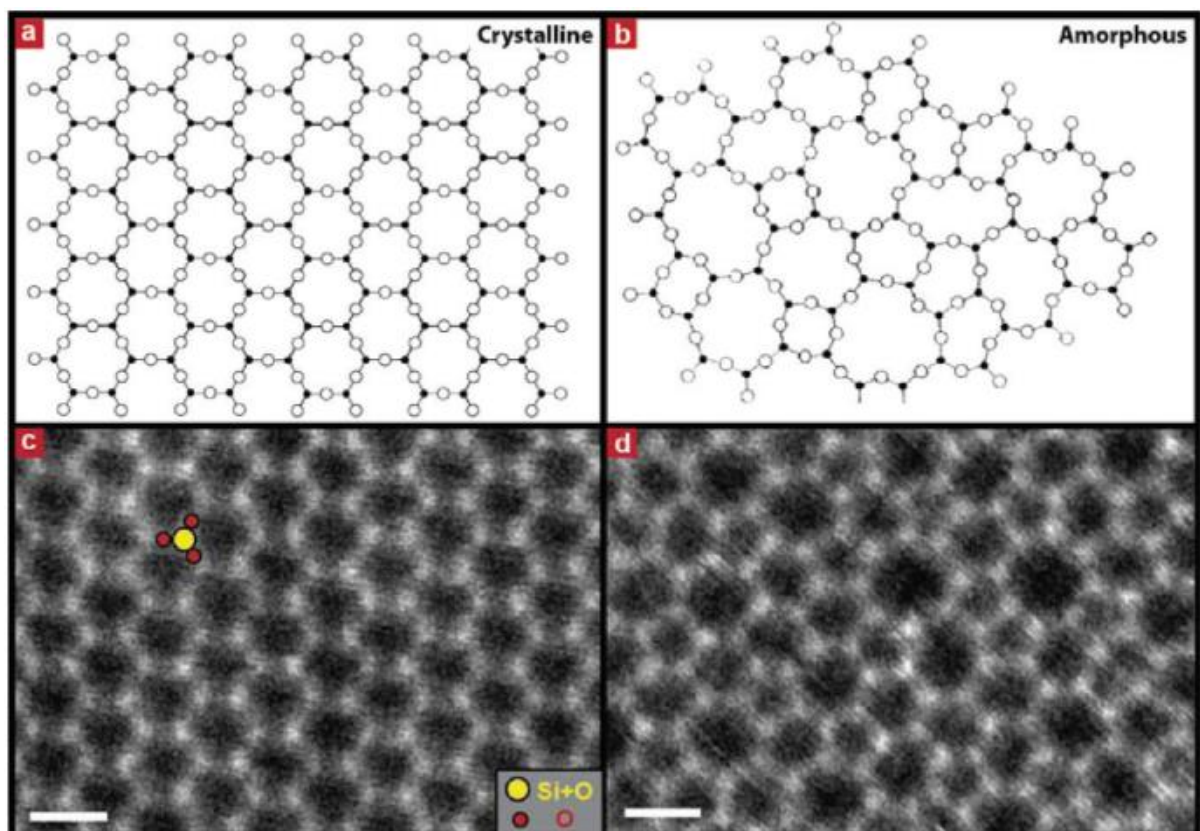


**Figure 3.** Atomic-resolution images of a 2D glass. (a,b) Zachariasen's models for a 2D crystal and a 2D amorphous glass. (c,d) Experimental TEM images of 2D crystalline and amorphous silica supported by graphene.[32]

In 2012, P. Y. Huang et al. [32] and M. Heyde et al. [33] demonstrated the atomic structure of a two-dimensional silica glass supported on graphene using

transmission electron microscopy (TEM), which emphasizes Zachariasen's accurate, insightful, and pioneering spirit. Transmission electron microscopy (TEM) experimental findings, as presented in Figure 3, closely resembled the picture proposed by Zachariasen 80 years earlier in 1932. The strong qualitative resemblance of these images to Zachariasen's model indicates that they show a 2D glass that approximately complies with the continuous random network model.

In the years following Zachariasen's publication, new definitions were proposed. These were based on the non-crystalline properties of glasses, their viscosity, and the glass transition. There are several definitions for glasses found in the literature:

“Glass is an X-ray amorphous material that exhibits the glass transition. This being defined as that phenomenon in which a solid amorphous phase exhibits with changing temperature (heating) a more or less sudden change in its derivative thermodynamic properties such as heat capacity and expansion coefficient, from crystal-like to liquid-like value”. J. Wong and C. Austen Angell, 1976[34]

“Glasses are amorphous materials that do not have long-range translational order (periodicity), characteristic of a crystal, with glass being an amorphous solid that exhibits a glass transition.” S. R. Elliott, 1989[35]

“A glass is a non-crystalline solid exhibiting the glass transition phenomenon.” J. Zarzycki, 1991[36]

“Glass is an amorphous solid. A material is amorphous when it lacks long-distance order, that is, when there is no regularity in the arrangement of molecular constituents, on a scale larger than a few times the size of these groups. No distinction is made between the words vitreous and amorphous.” R. H. Doremus, 1994[37]

However, these definitions are limited in several ways. The first one does not take into account glasses obtained by sol-gel or CVD (chemical vapor deposition). The second definition would emphasize that glasses can be formed from any composition - theoretically - whether it be inorganic, organic, biological, or metallic.

It is worth mentioning that until now, there has been no consensus on whether glasses are solids or supercooled liquids with such high viscosity that they appear solid but flow over time. This theory originated from the observation of ancient medieval stained glass in Europe. It was noted that the bottom of stained-glass windows were thicker than the top, implying the glass might have flowed over the centuries. The discussion culminated in an article entitled "*Do cathedral glasses flow?*" written by Edgar D. Zanotto [38]. Through viscosity measurements and calculations, they found that cathedrals' silica glasses would require  $10^{32}$  years to flow significantly. This period is significantly longer than the current age of the Universe ( $13.8 \times 10^9$  years). The thicker base of stained glass was one of the challenges in producing flat glass during the medieval period. When placing the glass in the window, artisans favored positioning its thickest part downwards to prevent breakage.

“Glass is an amorphous solid with complete absence of long-range order and periodicity, exhibiting a glass transition region. Any material, inorganic, organic or metal, formed by any technique, that exhibits a glass transition phenomenon is a glass.” J. E. Shelby, 1997[39]

Gupta[40] proposed that a non-crystalline solid (characterized by the presence of a halo on the X-ray diffractogram without any identifiable peaks) can be divided, from a thermodynamic standpoint, into two different categories: glasses and amorphous solids. Non-crystalline solids refer to materials that possess an extended and random three-dimensional network, i.e., characterized by a lack of symmetry and translational periodicity. From a thermodynamic perspective, a non-crystalline solid is considered a glass when it undergoes the glass transition phenomenon. As a result, amorphous solids can be classified as non-crystalline solids that do not manifest the glass transition. New definitions have been suggested to support this new classification:

“A glass is a non-crystalline solid, therefore, with absence of symmetry and translational periodicity, which exhibits the phenomenon of glass transition, and can be obtained from any inorganic, organic or metallic material and formed through any preparation technique.” O. L. Alves, I. F. Gimenez and I. O. Mazali, 2001[41]

“Glass is a solid having a non-crystalline structure, which continuously converts to a liquid upon heating.” Arun K. Varshneya, 2012[42]

We finally arrived in 2017, when the researchers Edgar D. Zanotto and John C. Mauro published the article “*The glassy state of matter: Its definition and ultimate fate*”[43], in which they revised the old definitions and created a new, more comprehensive one, with a focus on both researchers in the field and the lay public:

“Glass is a nonequilibrium, non-crystalline condensed state of matter that exhibits a glass transition. The structure of glasses is similar to that of their parent supercooled liquids (SCL), and they spontaneously relax toward the SCL state. Their ultimate fate, in the limit of infinite time, is to crystallize”. Edgar D. Zanotto and John C. Mauro, 2017

Theoretically, any substance can be turned into glass, as long as we can cool it from a liquid or gaseous state at such a high rate that the atoms and molecules that make it up do not have enough time to arrange themselves into organized structures that are thermodynamically more stable. As Varshneya concludes, “*the kinetic theory of glass formation does not address the question as to what structural characteristics of substances encourage ready glass formation. It assumes that all substances can be brought into glassy state. The only question it addresses is what minimum cooling rate is required to avoid a perceptible degree of crystallization*”[42]. Each substance has its own properties, so the cooling rate can be very different from one substance to another. For example, for liquid water to turn into glass, the cooling rate must be  $10^7 \text{ K} \cdot \text{s}^{-1}$ ,

while for silica this rate is  $0.9 \times 10^{-6} \text{ K} \cdot \text{s}^{-1}$ , which makes obtaining glasses of water more expensive and requires more specific techniques, in addition to limiting the size of the bulk, as there is a temperature gradient during the cooling process[44].

### 1.3. Glass formation from a melt.

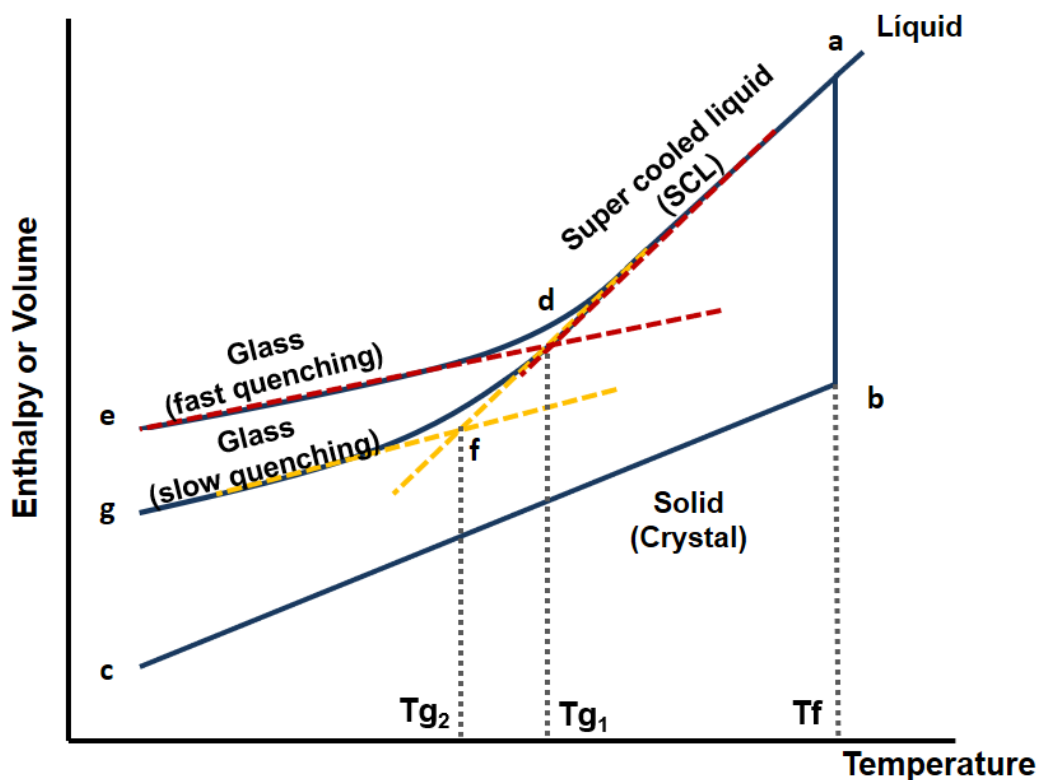
Traditionally, conventional glasses are produced using the melting/quenching method. This method includes the melting of a mixture of initial materials, typically at high temperatures until they turn into a homogenous liquid. Then, the mixture is rapidly cooled to increase its viscosity and maintain its non-crystalline characteristic. The structures of the raw material of a glass are similar to a liquid when melted. As cooling occurs, and its viscosity increases, the molten material can follow different structural patterns based on the cooling rate used.

Figure 4 shows the volume-temperature (V-T) diagram for a glass-forming liquid. According to the diagram, starting from high to low temperatures, we have the *abc* path, which shows the natural path for crystal formation. When we reach the melting temperature (or melting point, freezing temperature)  $T_f$ , we have an abrupt change in volume (or enthalpy) and, finally, the crystal is formed, being the lowest energy level of the compound itself. However, it is possible to cool liquids at temperatures below  $T_f$ . This metastable condition is known as super cooled liquids (SCL). It is important to point out that as the temperature decreases, the viscosity of the SCL increases proportionally. If this cooling is faster, we have the *ade* path. The gradual increase in viscosity occurs until the SCL does not flow, forming the glass. The transition from the SCL to the glass is instituted when the viscosity reaches the value of  $10^{14} \text{ Pa}\cdot\text{s}$ . The temperature at which this transition occurs is defined as the glass transition temperature ( $T_g$ ). As observed in the *afg* path, if the cooling rate occurs more slowly, the viscosity increases in the same proportion, forming a different glassy phase, with a different  $T_g$ , density and enthalpy, starting from the same initial liquid.

The  $T_g$  represents the temperature range where structural relaxation starts ( $10^{14} \text{ Pa}\cdot\text{s}$ ), transitioning from the glassy to the viscoelastic state. At this stage, certain properties such as viscosity, heat capacity, and thermal expansion begin to behave

differently than previously observed. Structural relaxation arises from unobstructed translational movements of chains relative to one another.

It is imperative to note that the V-T diagram is solely applicable to glasses created through melting-quenching. For instance, in the sol-gel process which achieves glasses from solutions at room temperature, and is a method unsuitable for V-T diagram application.



**Figure 4.** The volume-temperature diagram for a glass-forming liquid. *abc* path is related to the transition from a liquid to a conventional solid, with the transformation taking place at the melting point. *ade* path corresponds to a decrease in temperature and increase in viscosity of the liquid, becoming a supercooled liquid, and finally, with a sudden decrease in temperature and increase in viscosity, forming a glass. *afg* path corresponds to the same transformation, but with faster quenching. (Adapted from [43]).

## 2. MAGNETO-OPTICAL PROPERTIES

### 2.1 Brief history of magnetism and magneto-optical effect.

Magnetic phenomena have been present since the beginning of humanity. According to Roger Elliot: “*magnetism provides a particularly good example of the way in which the exact sciences have developed*”[45]. Magnetism was already known by the ancient Sumerians, Greeks, Chinese and America pre-Columbian people for millennia and interpreted it as magic. The name “*magnetic*” has its Greek origin, coming from the ferromagnetic stones extracted from the region of Magnesia, which became known as magnetites (from Greek μαγνήτις [λίθος] - magnētis [lithos] - meaning “[stone] from Magnesia”)[45,46].

During the Middle Ages, the Chinese developed the compass, a maritime instrument that was very relevant to the Chinese discoveries in the 15th century and the Iberian discoveries in the 16th and 17th centuries. In 1600, the Englishman William Gilbert (1544–1603) wrote *De Magnete, Magneticisque Corporibus, et de Magno Magnete Tellure* (On the Magnet and Magnetic Bodies, and on That Great Magnet the Earth), which is known to be the first scientific study on magnetism. In his work, Gilbert suggests that the Earth also operates as a large magnet [47].

In 1820, Hans-Christian Ørsted (1777-1851), a Danish physicist, observed that a defect occurred in a compass that was accidentally placed near his experiment while he was studying electricity and applied a current to metallic wires. This provided evidence that there was a physical relationship between electricity and magnetism. The unit of magnetic induction (Oe, oersted) in the centimeter-gram-second system (CGS) is named after Ørsted due to his contributions to the field of electromagnetism[47].

At the Royal Society in London, Humphry Davy (1778-1829) and William Hyde Wollaston (1766-1828) attempted to create an electric motor using magnets after learning of Ørsted's work, but it was Davy's student, Michael Faraday (1791-1867), who succeeded in creating the motor by using a steel magnet, a current-carrying wire, and a container of mercury as early as 1821. Faraday publicized his results in excitement without giving credit to Wollaston or Davy, causing controversy within the Royal Society. The controversy strained Faraday's relationship with his mentor Davy and possibly led to his assignment to other pursuits by the Royal Society. Faraday resumed his work on magnetism only after Davy's death years later[47,48].

In 1845, Faraday demonstrated that it was possible to change the plane of polarization of a beam of light when this beam passed through a specific medium (in this case, a glass containing PbO with a high refractive index) under a magnetic field application, parallel to the direction of light propagation. This effect became known as the Faraday effect, the first of the discovered magneto-optical effects[49,50]. Showing the relevance of this discovery, the Faraday effect proved that light is an electromagnetic radiation, mathematically demonstrated in 1864 by James Clerk Maxwell, unifying the theories of electricity, magnetism and light, which is summarized in the four famous equations that bear his name:

$$\oint \vec{E} \cdot d\vec{A} = \frac{q}{\epsilon_0} \quad \text{Gauss's Law} \quad (\text{Eq. 1})$$

$$\oint \vec{B} \cdot d\vec{A} = 0 \quad \text{Gauss's law for magnetism} \quad (\text{Eq. 2})$$

$$\oint \vec{E} \cdot d\vec{s} = - \frac{d\Phi_B}{dt} \quad \text{Faraday's law of induction} \quad (\text{Eq. 3})$$

$$\oint \vec{B} \cdot d\vec{s} = \mu_0 \epsilon_0 \frac{d\Phi_E}{dt} + \mu_0 i \quad \text{Ampère's circuital law} \quad (\text{Eq. 4})$$

where  $\vec{E}$  is electric field,  $\vec{B}$  is the magnetic field,  $d\vec{A}$  is the differential surface vector,  $d\vec{s}$  is the differential length vector,  $q$  is the charge,  $\epsilon_0$  is the vacuum electric permeability,  $\mu_0$  is the vacuum magnetic permeability,  $d\Phi_B$  is the magnetic flux,  $d\Phi_E$  is the electric flux,  $dt$  is the time and  $i$  the unit imaginary number[47].

In 1877, the Scottish physicist John Kerr (1824–1907) managed to change the polarization of a beam of light by reflection, under a magnetic field, which became known as the magneto-optical Kerr effect (MOKE)[51,52]. Over time, new magneto-optical effects were discovered and described, such as for example the Zeeman, Voigt, Cotton–Mouton and inverse Faraday effects[53–55]. From now on, we will focus on the magneto-optical Faraday effect, which will be explored in this work.

## 2.2. Magnetism in atoms and macroscopic magnetic properties of materials.

Magnetic susceptibility ( $\chi$ ) is a measure of the magnetizing strength of a material in an applied magnetic field. It is the ratio of the magnetization  $\mathbf{M}$  (magnetic moment per unit volume) to the strength of the applied external magnetic field  $\mathbf{B}$ , as shown in Eq. 5 below. This allows a simple classification of the response of most materials to an applied magnetic field: aligned with the magnetic field and being attracted by it,  $\chi > 0$ , called paramagnetic, or non-aligned with the magnetic field, being repelled,  $\chi < 0$ , called diamagnetic.

$$\chi = \frac{M}{B} \quad (\text{Eq. 5})$$

These magnetic properties are intrinsic to all matter and come from the filling of electrons in the valence layers, that is, from the total angular momentum of an atom (or ion, or molecule), resulting from the coupling of magnetic ( $m_\ell$ ) and spin ( $s$ ) quanta number. For half-filled orbitals, the unpaired electrons line up with  $\mathbf{B}$  and are attracted to it. As for orbitals with fully paired electrons, there is a resistance for these electrons to pair with the field, being repelled by it. This comes from the **Pauli exclusion principle** and the **Hund's rule of maximum multiplicity**. The Pauli Principle allowed each orbital to accommodate a maximum of 2 electrons at the same time, as long as they had opposite spin signals, which became known as paired electrons. According to this Principle, no two particles can have the same set of four quantum numbers in the same system. Hund's rule also facilitated the study of polyelectronic orbitals, proposing that the energy of a subshell is lowest when the orbitals are half-filled and, therefore, it is energetically preferable for atoms to be in their lowest energy state, the ground state. The Bohr–Van Leeuwen theorem proves that every sort of magnetism is impossible for electrons in classical physics, being totally dependent on states and quantum numbers.

It is important to note that most atoms have at least one filled orbital, so the sum of paramagnetic ( $\chi_{\text{para}}$ ) and diamagnetic ( $\chi_{\text{dia}}$ ) susceptibility is present in materials. Unlike paramagnetism, diamagnetism is a property of all atoms in a molecule. While paramagnetism is caused by the presence of unpaired electrons in the molecule, all electrons, whether paired or unpaired, induce diamagnetism. The conflict between

paramagnetism and diamagnetism defines the total (measured) magnetic susceptibility  $\chi_{\text{meas}}$ , which is positive for paramagnetic materials and negative for diamagnetic materials. Diamagnetic effects are temperature independent and are naturally orders of magnitude smaller,  $\sim 10^{-6}$  emu.mol $^{-1}$ , than paramagnetic effects,  $\sim 10^{-2}$  emu.mol $^{-1}$ . Figure 5 shows the resulting molar magnetic susceptibility for each atom. It is possible to analyze that certain elements have dominant diamagnetic values, and, for others, dominant paramagnetic values. Fe, Co, and Ni atoms naturally have high  $\chi$  values (1-10 emu.mol $^{-1}$ ), which promotes ferromagnetic effects.

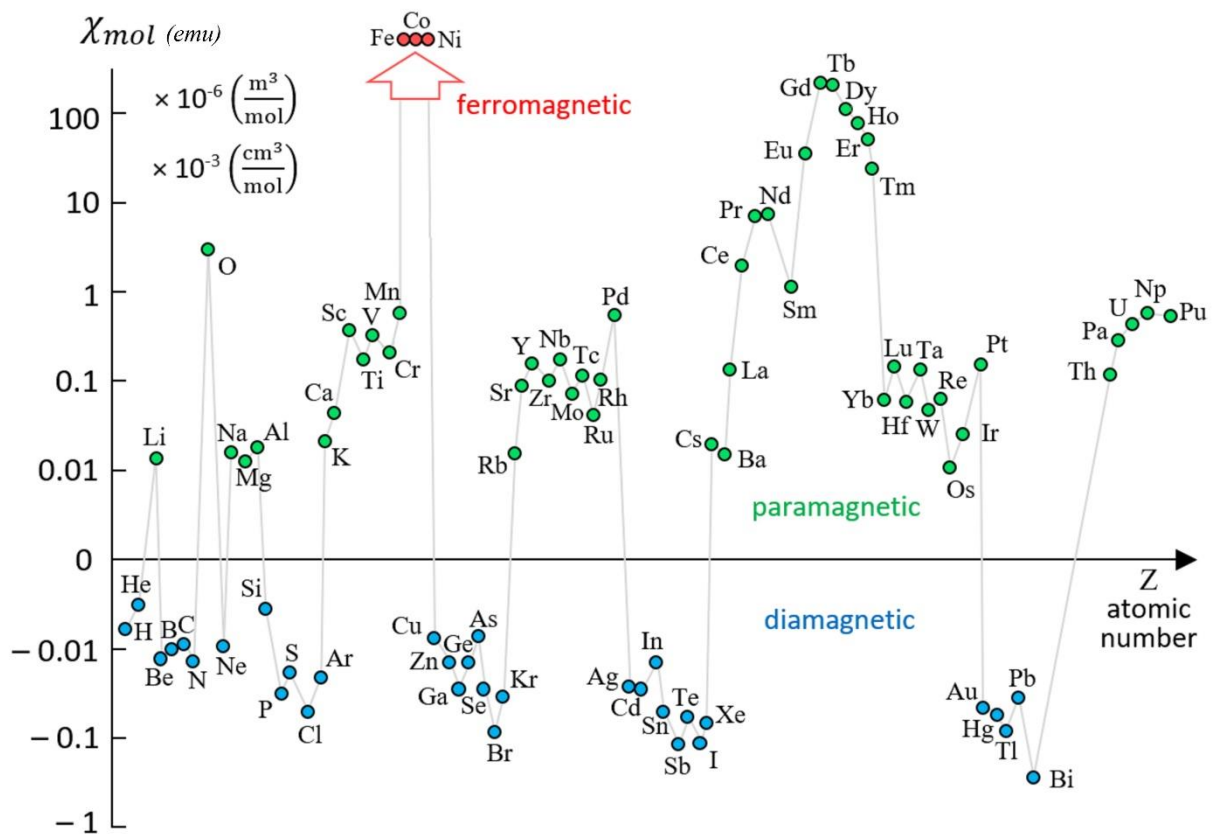


**Figure 5.** Variation of molar susceptibility for each atom. For some, the diamagnetic effect is dominant, mainly due to the filling of the valence orbitals. Negative values indicate that they are repelled by the external magnetic field,  $B$ . For others, the paramagnetic effect is the most relevant, due to the number of half-filled orbitals. Positive values show that they are attracted by  $B$ . Fe, Co and Ni atoms have naturally high susceptibility, promoting ferromagnetic characteristics [Figure from Stan Zurek, Magnetic susceptibility, Encyclopedia Magnetica].

The works of Paul Pascal[56–59] proposed that the diamagnetism of a molecule could be determined in an additive fashion using values for the diamagnetic susceptibility of every atom ( $\chi_{Di}$ ) and bond ( $\lambda_i$ ) in the molecule, as show in Eq. 6

$$\chi_{dia} = \sum_i \chi_{Di} + \sum_i \lambda_i \quad (Eq. 6)$$

Table 1 contain pre-determined  $\chi_{dia}$  values for important groups of atoms or ions. These will be the values that will be used to determine the theoretical  $\chi_{dia}$  of the glasses produced in this work and, from the  $\chi_{meas}$ , determine the  $\chi_{para}$ .

**Table 1.** Theoretical values of  $\chi_{dia}$  for some ions[59].

<b>Ion</b>	<b>O<sup>2-</sup></b>	<b>B<sup>3+</sup></b>	<b>W<sup>6+</sup></b>	<b>Tb<sup>3+</sup></b>	<b>Sb<sup>3+</sup></b>
$\chi_{dia}$ (x 10 <sup>-6</sup> emu . mol <sup>-1</sup> )	-12	-0.2	-13	-19	-17
<b>Ion</b>	<b>P<sup>5+</sup></b>	<b>Pb<sup>2+</sup></b>	<b>Zn<sup>2+</sup></b>	<b>Mn<sup>2+</sup></b>	<b>Mn<sup>3+</sup></b>
$\chi_{dia}$ (x 10 <sup>-6</sup> emu . mol <sup>-1</sup> )	-1	-32	-15	-14	-10
<b>Ion</b>	<b>Sm<sup>3+</sup></b>	<b>Eu<sup>3+</sup></b>	<b>Gd<sup>3+</sup></b>	<b>Dy<sup>3+</sup></b>	<b>Ho<sup>3+</sup></b>
$\chi_{dia}$ (x 10 <sup>-6</sup> emu . mol <sup>-1</sup> )	-20	-20	-20	-19	-19

As stated earlier, paramagnetic effect arises from the interaction of B with the magnetic field of the unpaired electrons due to the coupling spin (S) and orbital angular momenta (L), the total angular momentum (J). Spin angular momentum is given by the product of the electron's spin quantum number and the Planck constant (h) divided by  $2\pi$ ,  $\hbar$ . The spin quantum number can take on two possible values: +1/2 or -1/2, corresponding to the two possible orientations of the electron's spin, as show in Eq. 7.

$$\mathbf{S} = \left| \sum_{i=1}^n s_i \right| ; \quad \mathbf{L} = \left| \sum_{i=1}^n l_i \right| ; \quad \mathbf{J} = (\mathbf{L} + \mathbf{S}) \quad (Eq. 7)$$

The orbital angular momentum (L) of an electron is given by the product of its orbital radius, its momentum, and the sine of the angle between its momentum vector and the radial vector pointing from the electron to the nucleus. This angular momentum can take on discrete values, determined by the principal quantum number (n), which is related to the shape of the electron's orbit. The possible values of l range from 0 to n-1, where n is the principal quantum number that specifies the energy level of the electron. The total angular momentum (J) is rise to several J –states, ranging  $|L + S| \leq J \leq |L - S|$ .

For paramagnetic effects, the magnetization M is directly proportional to an applied magnetic field B. However, if the material is heated, this proportionality is reduced. For a fixed field value,  $\chi_{para}$  is inversely proportional to temperature, as shown in Eq. 8, called Curie's Law. The relation between  $\chi$  and temperature was studied and postulated in the doctoral thesis of the French physicist Pierre Curie (1859–1906), entitled “*Propriétés magnétiques des corps à diverses températures*” in 1895[60].

$$\chi_{para} = \frac{M}{B} = \frac{C}{T} \quad (Eq. 8)$$

where T is temperature (K) and C is a material-specific Curie constant ( $A.m^2.T^{-1}.mol^{-1}$ ).

Curie constant will depend on the J, which in turns depends on the atom (or ion, or molecule) ground state of each ion. Eq. (9) shows respectively those relations.

$$C = \frac{N_A \mu_B^2}{3 k_B} \cdot \mu_{eff}^2 = \mathbf{5/4} \cdot g_J^2 [J(J + 1)] \quad Eq. (9)$$

in red,  $N_A$  is the Avogadro constant ( $6.022 \times 10^{23} mol^{-1}$ ),  $k_B$  is the Boltzmann constant ( $1.380 \times 10^{-23} J.K^{-1}$ ),  $\mu_B$  is the electron's intrinsic magnetic moment, known as Bohr magneton ( $e\hbar/2m_e = 9.274 \times 10^{-24} A.m^2$ ). The ratio of these three constants is equal to the result **5/4** ( $A.m^2.T^{-1}.mol^{-1}$ ) or **1/8** ( $emu.Oe^{-1}.mol^{-1}$ ). the disordered state total magnetic moment,  $\mu_{eff}$ , is dependent on J and the Landé g-factor,  $g_J$ , which is also a term dependent on the ground state of each ion, as shown in the Eq. (10).

$$g_J = 1 + \frac{J(J + 1) + S(S + 1) - L(L + 1)}{2J(J + 1)} \quad \text{Eq. (10)}$$

It is possible to obtain the value of the Curie constant experimentally, observing the variation of the susceptibility varying the temperature, under a constant applied magnetic field. Figure 6a shows illustratively the variation of magnetic susceptibility with temperature, under constant B.  $\chi_{\text{dia}}$  is not affected by temperature, but  $\chi_{\text{para}}$  increases exponentially at T close to 0 K. Inset shown the inverse of susceptibility ( $1/\chi_{\text{para}}$ ) versus temperature, varying linearity. The slope of this linear variation will be the value of the Curie constant. If the measured substance exhibits this linear behavior under  $1/\chi_{\text{para}}$ , it has paramagnetic interactions and follows Curie's law.

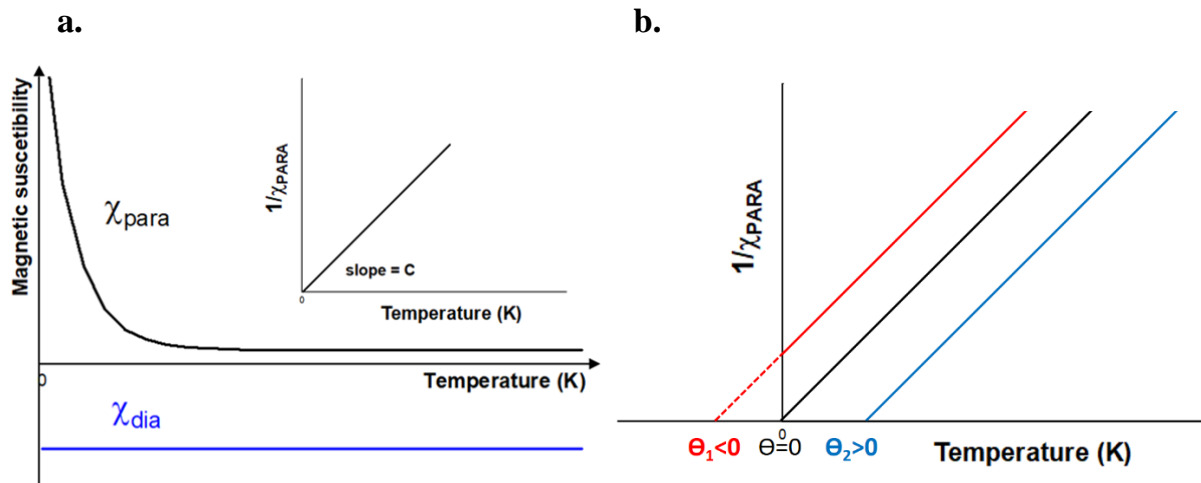


**Figure 6.** (a) Paramagnetic (black) and diamagnetic (blue) susceptibility versus temperature under constant applied magnetic field. Inset of shown the inverse of paramagnetic susceptibility versus temperature, varying linearity. (b) Curie's law deviation, with three different Weiss temperatures,  $\theta < 0$ ,  $\theta = 0$  and  $\theta > 0$ . [Adapted from [47]]

As observed in Figure 6b, some substances present a deviation in Curie's law. They still have the linear behavior for  $1/\chi_{\text{para}}$ , but the intercept is not exactly at 0 K, it can be before, or even after (using projection, since there are no values below 0 K). This effect occurs because there are interatomic interactions between moments, causing parallel or antiparallel spin alignments. This effect was added to Curie's law as the

correction constant  $\theta$  (K), known as the Weiss Temperature, as shown in Eq. 11, the Curie–Weiss law, named in honor to Pierre-Ernest Weiss (1865–1940), who studied these effects[61].

$$\frac{1}{\chi_{para}} = \frac{1}{C}T + \left(-\frac{\theta}{T}\right) \quad (Eq. 11)$$

For  $\theta = 0$  K, there are no interactions of interatomic spins and the equation becomes equal to Eq. 8. Now for,  $\theta > 0$  K, the spins are aligned parallel, causing low ferromagnetic interactions. If  $\theta < 0$  K, the spins are aligned antiparallel, causing low antiferromagnetic interactions. It is important to note that these interactions are insignificant compared to the paramagnetic effect and the ferromagnetism or antiferromagnetism effects have completely different behavior under the same conditions.

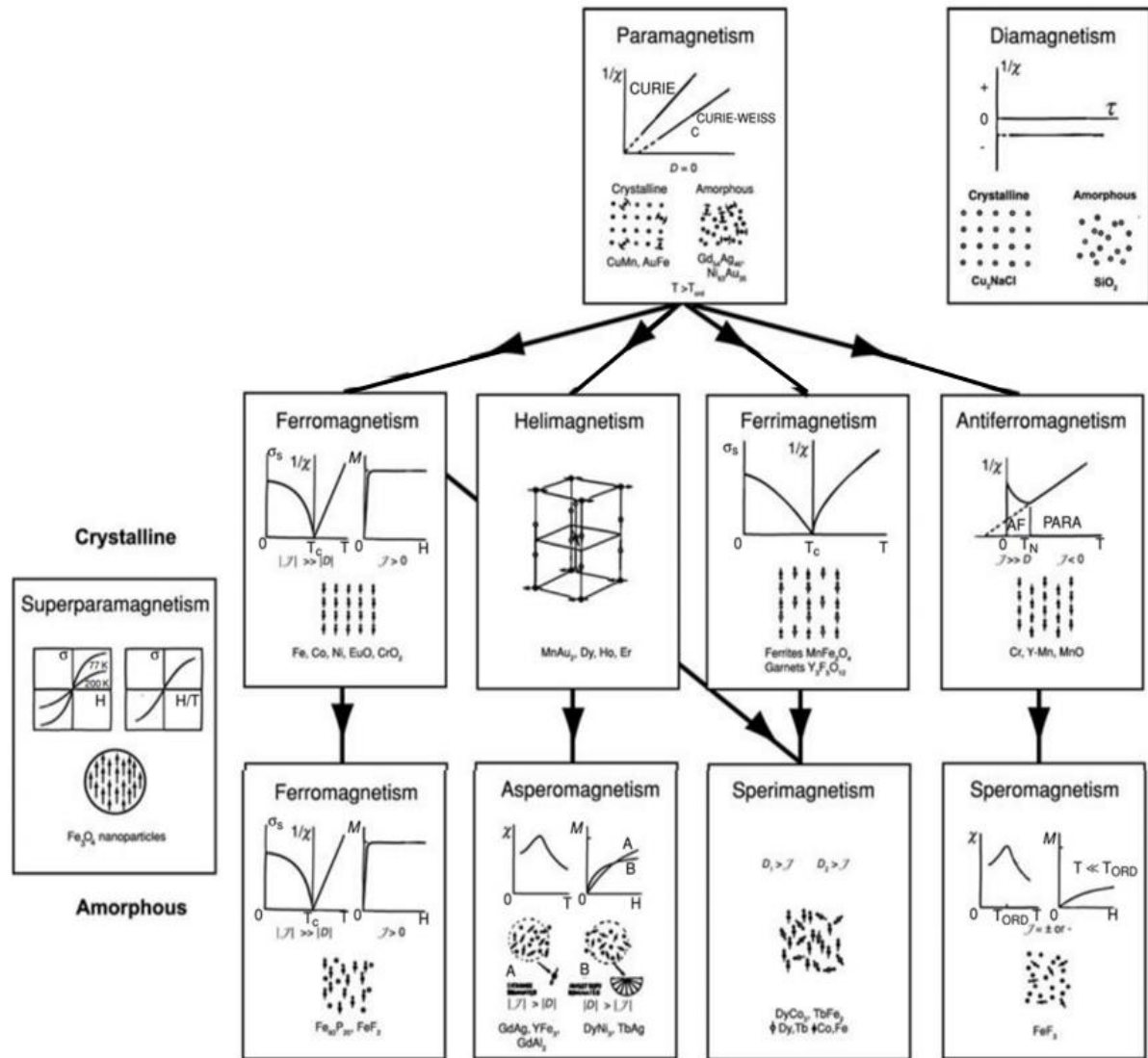


**Figure 7.** The magnetic family tree, showing the evolution of macro-magnetic properties, the behavior of magnetic susceptibility, the organization of spins and some examples of substances that have these effects, making clear the complexity of magnetic effects[47].

Now we can talk a little about the other magnetic effects. As seen in Figure 7, macroscopic magnetic effects arise from paramagnetism. It is present the names of the effects, the behavior of substances with this effect when we modify B or the temperature, drawings representing the ordering of spins, in addition to mentioning some compounds that present such effects. The most known are ferromagnetism, antiferromagnetism and ferrimagnetism, which differ in the way that the magnetic moments of atoms in a material are arranged.

Ferromagnetism is the most familiar type of magnetism, where the magnetic moments of the atoms are aligned parallel to each other within each domain, resulting in a net magnetic moment for the entire material. When an external magnetic field is applied, the magnetic domains become aligned with the field, leading to a strong attraction between the material and the magnetic field. They can be artificially magnetized applying a strong  $B$  for a period of time. It is observed in pure metals such as Fe, Ni and Co, as well as compounds such as  $\text{Fe}_3\text{O}_4$  (found in magnetite) and  $\text{Nd}_2\text{Fe}_{14}\text{B}$  (neodymium magnet).

Antiferromagnetism, on the other hand, is observed in certain materials such as chromium and manganese oxide. In antiferromagnetic materials, the magnetic moments of adjacent atoms are aligned in opposite directions, resulting in a net zero magnetic moment for the entire material. When an external magnetic field is applied, the magnetic moments become aligned with the field in a way that cancels out the overall magnetic moment of the material, leading to little or no attraction between the material and the magnetic field.

In ferrimagnetic materials, the magnetic moments of atoms in different sublattices are aligned parallel to each other, but the moments in different sublattices are oriented in opposite directions. This results in a net magnetic moment for the material, but it is smaller than in ferromagnetic materials. Ferrimagnetism is a complex phenomenon that arises from the competition between ferromagnetic and antiferromagnetic interactions within the material. This type of magnetism is observed in materials such as ferrites and garnets.

By raising the temperature of the substance, the ferromagnetic effect is lost, becoming the pure paramagnetic effect. The temperature at which this change occurs is called the Curie temperature,  $T_C$  (K). The same occurs for ferrimagnetic and antiferromagnetic substances. With increasing temperature, there is a transition from the effect in question to the paramagnetic effect. This temperature where the transformation of effects occurs is called the Néel temperature,  $T_N$  (K). Figure 8a illustrates the variation of magnetic susceptibility with temperature for hypothetical substances. Ferromagnetic and antiferromagnetic effects are present up to  $T_C$  and  $T_N$ , respectively. At higher temperatures, substances exhibit only the paramagnetic effect. Figure 8b. shows the

behavior of the same substances on a plot of the inverse of magnetic susceptibility versus temperature. Figure 8c. shows a representation of the spin alignments for these three substances, with parallel alignment in favor of the external field in for ferromagnets, antiparallel alignment, resulting in a null effect, for antiferromagnets, and an antiparallel alignment for ferrimagnets, but with differences in intensity between the spins ( $A > B$ ) in the direction of external magnetic field, resulting in a non-zero effect, but smaller than for ferromagnets.

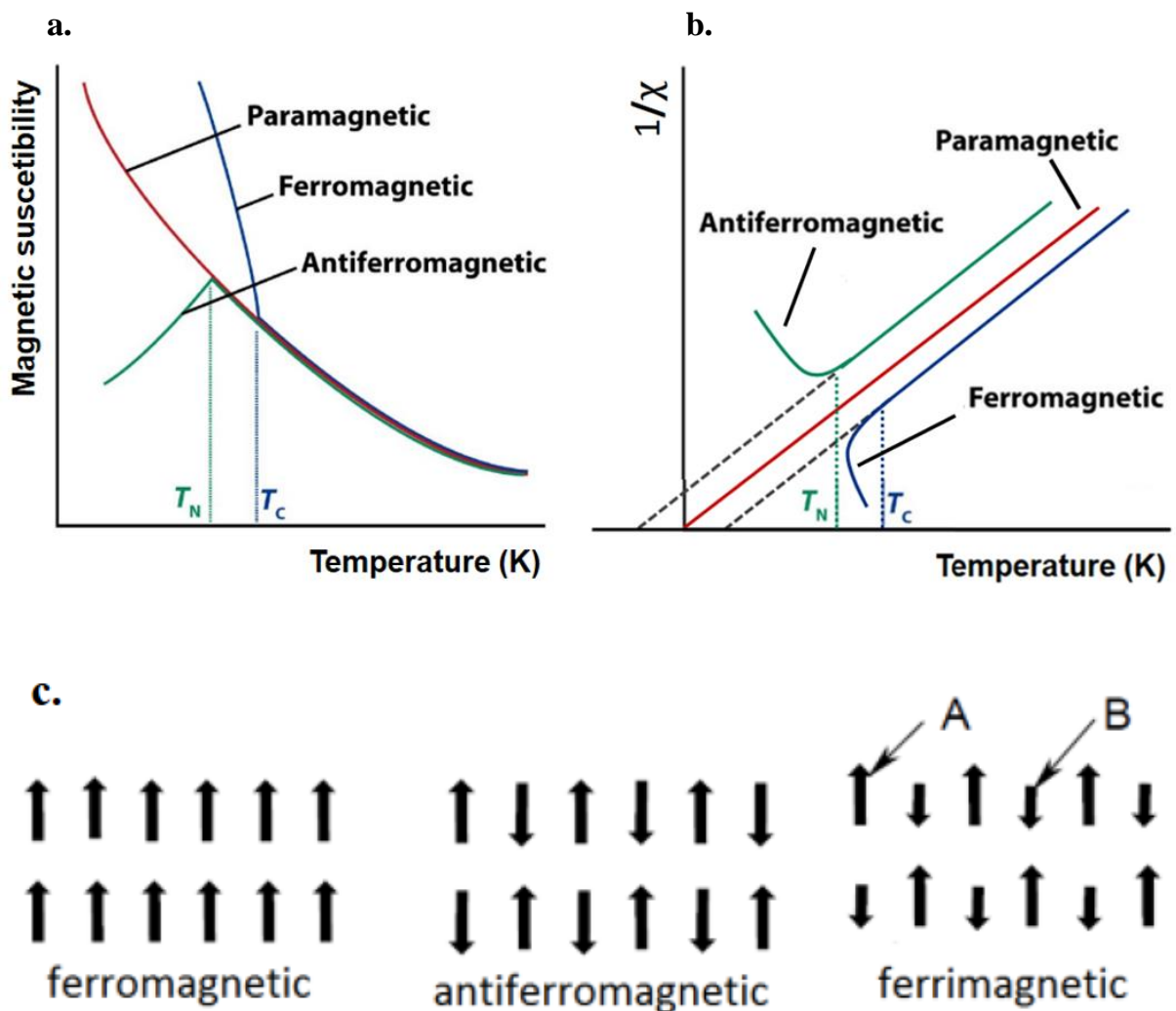


**Figure 8.** Behavior of (a) magnetic susceptibility and (b) of the inverse magnetic susceptibility for paramagnetic (red), ferromagnetic (blue) and antiferromagnetic (green) substances with temperature variation, under constant external magnetic field, showing  $T_C$  and  $T_N$ . (c) Representation of spin alignment for ferromagnetic (parallel alignment), antiferromagnetic

(antiparallel alignment) and ferrimagnetic (antiparallel alignment with differences in intensity A and B) substances. [Adapted from [47]

Helimagnetism effect occurs when, at certain temperatures, ferromagnetic layers couple ferromagnetically to the neighboring layers, but antiferromagnetically to the next-neighbour layers forming a helical spin structure. Examples of substances with this effect are FeGe (< 278 K), Tb (219-231 K) and  $\beta$ -MnO<sub>2</sub> (< 93 K)[47].

Superparamagnetism occurs in sufficiently small ferromagnetic or ferrimagnetic nanoparticles. The magnetization can randomly reverse direction under the influence of temperature (also called Néel temperature). In the absence of an external magnetic field, their magnetization appears to be zero on average. In this state, called superparamagnetism, an external magnetic field can magnetize the nanoparticles in a manner similar to that of a paramagnet. However, their magnetic susceptibility is much greater than that of paramagnets. An example is ZnFe<sub>2</sub>O<sub>4</sub> nanoparticles[62,63].

When an antiferromagnetic response is observed for  $\chi$  versus temperature curves, but the substance lacks a crystalline lattice, the effect is called speromagnetism or asperomagnetism. They are distinguished by the length scale over which the spin correlations reach zero. In a speromagnet, the average spin correlations are negative at nearest neighbor but tend to zero at some interatomic distances. In an asperomagnet, the correlations are ferromagnetic and tend towards zero on a larger scale. In sperimagnetism, there is an order in most of the spins when B is applied, but there is an offset of other spins close to those aligned to the field[47,64].

Finally, another observed effect is the Pauli paramagnetism. Restricted to metals, this effect occurs due to the delocalization of electrons due to the formation of the metallic band, the free-electron model, and there is a mixture of excited states that are not filled, regardless of temperature.

### 2.3 Principles of the magneto-optical Faraday effect.

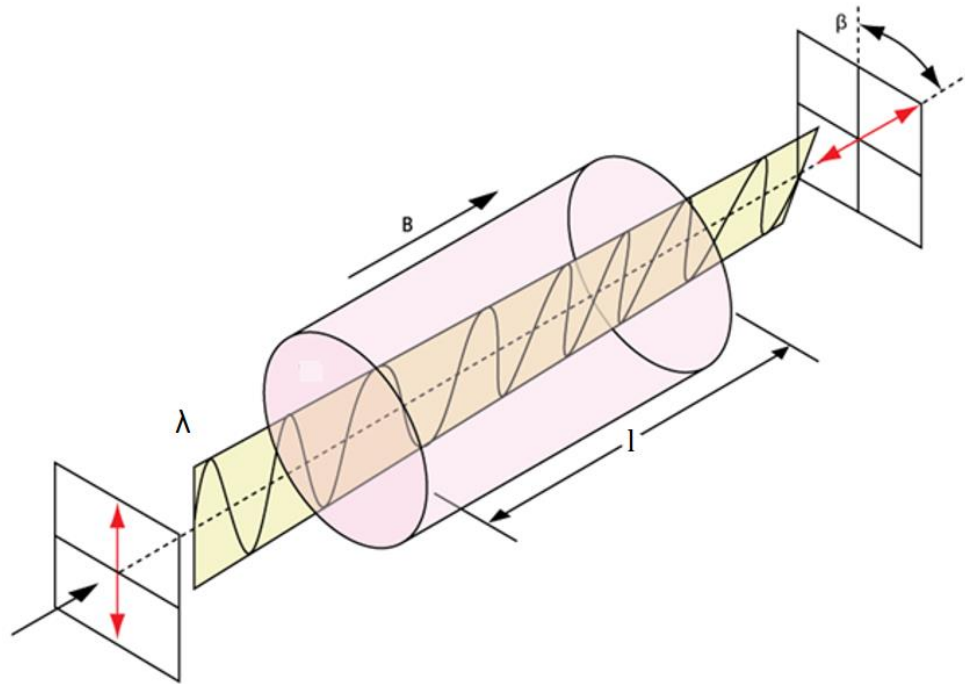


**Figure 9.** Schematic figure of a Faraday rotator. Polarizer light  $\lambda$  passes through the medium with optical path  $l$ , under the external magnetic field and constant  $B$ , causing a rotation of the plane of polarization of light, measured at angle  $\beta$ . [Extracted from ThorLabs – Faraday Rotators page. [https://www.thorlabs.com/images/TabImages/Faraday\\_Rotator\\_Diagram\\_D1-780.gif](https://www.thorlabs.com/images/TabImages/Faraday_Rotator_Diagram_D1-780.gif)]

As previously mentioned, and shown in Figure 9, the Faraday effect (or Faraday rotation) is a magneto-optical phenomenon (MOFE) which a change in the polarization plane of light occurs when passing through a medium, under the application of an external magnetic field,  $B$ . These conditions produce circular birefringence along  $B$  axis, resulting in a rotation of the polarization direction. The materials that have this effect are called Faraday rotators.

Already in Faraday's observations, in 1845, it was clear that the effect proportionally depended on some parameters such as the intensity of  $B$ , the size ( $l$ ) and the index of refraction ( $n$ ) of the transparent material. They have been summarized in Eq. 12 below.

$$\beta = V \cdot B \cdot l \quad (\text{Eq. 12})$$

where  $\beta$  is the angle of rotation, and  $V$  an intrinsic constant of each material, dependent on the refractive index, called Verdet constant ( $\text{min.Oe}^{-1}.\text{cm}^{-1}$  or  $\text{rad.T}^{-1}.\text{m}^{-1}$ ).  $B$  can occur clockwise, in this case the angle assumes a negative value, or counterclockwise, in this case assuming a positive value. Eq. 13 and 14 presents the dependencies of Verdet constant, that can be evaluated by constant presents diamagnetic ( $V_{\text{dia}}$ ) and paramagnetic ( $V_{\text{para}}$ ) contributions, respectively. If the resulting effect is diamagnetic,  $\beta$  will be positive. If the resultant is paramagnetic, the  $\beta$  will be negative.

$$V_{\text{dia}} = \left( \frac{ev}{m_e c} \right) \frac{dn}{dv} \quad (\text{Eq. 13})$$

where  $e$  is the elementary charge ( $1.602176634 \times 10^{-19}$  C),  $m_e$  is the mass of the electron ( $9.1093837015 \times 10^{-31}$  kg),  $c$  is the speed of light ( $299792458$  m.s<sup>-1</sup>),  $v$  is the frequency of the incident light, and  $dn/dv$  is the refractive index dispersion. This equation was derived by Antoine Henri Becquerel (1852-1908) on the basis of classical electromagnetic theory[65–67].

$$V_{\text{para}} = \left( \frac{4\pi^2 \mu_B v^2}{3Tch k_B} \right) \frac{N_I \mu_{\text{eff}}^2}{g} \sum_n \frac{C_n}{(v^2 - v_n^2)} \quad (\text{Eq. 14})$$

where  $N_I$  is the number of paramagnetic species  $I$  per unit volume ( $\text{I} \cdot \text{cm}^{-3}$ ),  $C_n$  is related to the transition probabilities,  $v_n$  is the transition frequencies. The Faraday effect is related to the inequality of the refractive indices of the left and right circularly polarized components into which the incident light is decomposed. The Verdet constant is dependent on the wave frequency and the internal resonance frequencies related to the transitions between electronic levels that are influenced differently by left and right circularly polarized waves, as well as on the associated transition probabilities. The Eq. 14 was studied and proposed by J. H. van Vleck and M. H. Hebb[68–70] and we can rearrange it as a function of  $\chi_{\text{para}}$  using Eq. 8 and 9., forming Eq. 15, below.

$$V_{para} = \left( \frac{4\pi^2}{ch\mu_B N_A} \right) \frac{N_R v^2}{g} \chi_{para} \sum_n \frac{C_n}{(v^2 - v_n^2)} \quad (Eq. 15)$$

where  $\frac{4\pi^2}{ch\mu_B N_A}$  is constant equal to  $3.558 \times 10^{25} \text{ mol.m.J}^{-1}.\text{A}^{-1}$ , independent of medium or light. We can conclude that  $V_{para}$  is directly proportional on  $\chi_{para}$  and its determination is extremely relevant for the study of paramagnet Faraday rotators, reaching higher Verdet constants and sensitivity orders of magnitude higher than diamagnetic Faraday rotators.

As seen in Eq. 13 and 15, the  $V$  is also dependent on the refractive index of the substance, due to the interaction of electromagnetic radiation with the molecular electric field. Therefore, larger, more polarizable atoms have greater interaction with electromagnetic radiation, with the electron cloud being more easily distorted. No wonder, the magneto-optical effect was discovered by chance by Faraday using a lead-borosilicate glass, where the presence of lead, a high polarizable atom, allowed the detection of the effect, despite being a glass with resulting diamagnetic susceptibility. The relationship between the  $V$  and the polarizability ( $\alpha$ ) can be better understood by means of the Eq. 16[20].

$$V = - \sum_n \frac{3I_n \alpha_n^2}{4r_n^6} \quad (Eq. 16)$$

where  $r_n$  is the distance between atoms and  $I_n$  is the ionization energy of which atom.

For MO materials, large angles of optical polarization rotation at wavelengths of interest as well as high optical transparency are generally required for use in photonic devices. This has been achieved by increasing the magnetic field intensity, increasing the path length in the material (like optical-fibers) or by developing new materials aimed at achieving higher  $V$ . Although any transparent materials under magnetic field exhibit some degree of Faraday rotation, only a few groups of substances can achieve large Faraday rotation angles and possess a high  $V$  for commercial applications in optics. Hence, the discovery of alternative high  $V$  materials for MO applications with inexpensive and abundant substances is a compelling technological opportunity for novel material innovation. Organic molecules containing aromatic

rings[71,72], polymers[73], and nanocomposite[74] have shown relevant results as MO materials in the visible and near infrared region, although the values are still low when compared to inorganic ones. Of these applications, the most commons are magnetic field sensors.

By far, the most frequent materials used in magneto-optical applications are single crystal materials based on inorganic garnets, as terbium gallium garnet (TGG), terbium aluminum garnet (TAG), rare earth iron garnets (RIGs), yttrium aluminum garnet (YAG), and other combinations of RE doped garnets, being commercially available, deployed in magneto-optical isolators and magnetic detection applications due to their high  $V$ , chemical stability and optical transparency in the region of interest. Garnets naturally have the general formula of  $X_3Y_2(\text{SiO}_4)_3$ , and synthetic garnets, mentioned above, were produced by replacing Si with Ga, Fe or Al. They are usually synthesized by Czochralski or Float Zone growth methods to produce high quality results without impurities or defects[75,76]. The  $V$  values for each single crystal is  $-134 \text{ rad.T}^{-1}.\text{m}^{-1}$  (TGG, at 632.8 nm),  $-174 \text{ rad.T}^{-1}.\text{m}^{-1}$  (TAG, at 632.8 nm),  $+5,86 \text{ rad.T}^{-1}.\text{m}^{-1}$  (YAG, at 632.8 nm),  $-232 \text{ rad.T}^{-1}.\text{m}^{-1}$  (YIG, at 1.86  $\mu\text{m}$ )[77].

As previously seen Fe, Ni and Co have high paramagnetic susceptibilities, which allows them to be excellent ions to work in MO applications. However, the presence of these ions causes unwanted coloration in the material, having, in most cases, applications only in the infrared region. The second group of atoms with high paramagnetic susceptibility are the rare earths. Because they have many unpaired electrons in the 4f layer, as is the case with Tb, Gd, and because they do not have high absorptions in the visible, these ions are also used commercially.

One of the biggest difficulties of monocrystalline Faraday rotators is their production. The production of single crystals is extremely costly, as all material must be grown without impurities or defects, or the effect will be impaired. moreover, production is limited by the size of the piece, as it usually only reaches a few mm in thickness. And, of course, this reverts to the final price of the product. Searching for prices on Faraday rotators by *Thorlabs, Inc.*, we will not find anything less than \$600.00 on rotators smaller than 5 mm.

Seeking to overcome this, the study of glasses with magneto-optical applications has been an increasing focus in modern science. Glasses have a synthesis advantage, as the melt-quenching method only requires increasing the temperature of the precursor reagents until melting, homogenization and thermal quenching at a lower temperature. In addition, it is possible to manufacture pieces larger than 5 mm, the major limitation being the region forming the glass in question. If glass production is satisfactory, it is possible to produce an optical fiber from it, and even if the  $V$  is not as high as that of the monocrystalline Faraday rotators, the  $l$  of an optical fiber would be an extra gain (as already seen in Eq. 12). These promises of new materials have called the scientific community, as will be discussed in the next section.

#### **2.4 State of the art of Faraday rotator glasses.**

A web search was conducted on the Web of Science on October 20, 2023, using the terms “*Magneto-optical sensors*” and “*Magneto-optical glasses*”, shown in Figures 10 and 11, respectively. The results showed a significant increase in publications and citations in recent years. The publication-citation records of 70-1400 and 47-1000 for the given date highlight the recent emergence, diversity, interest, and significance of these topics.

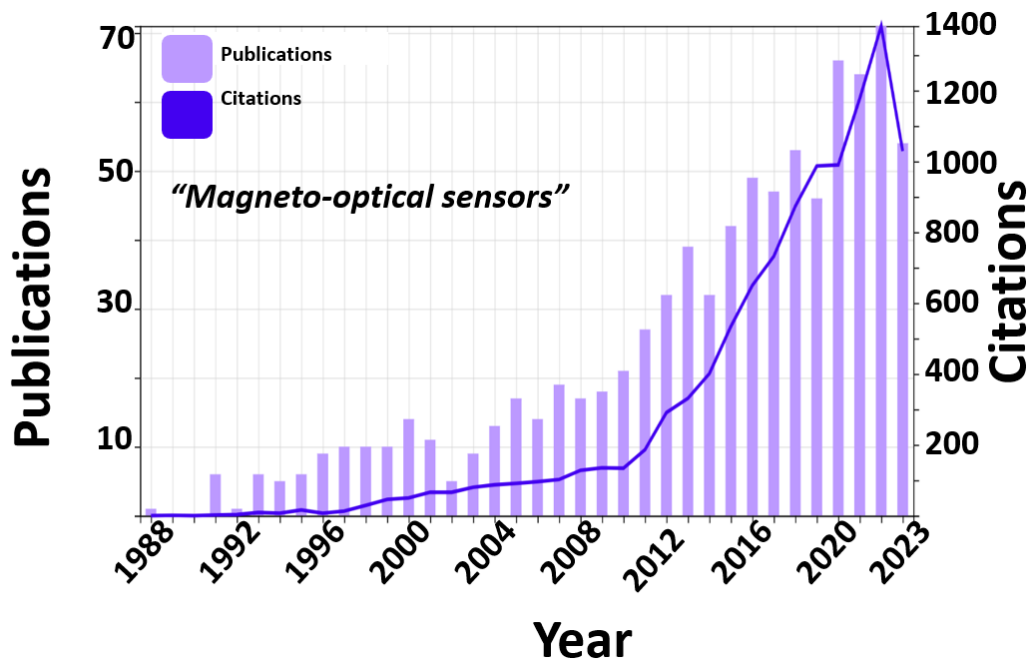


**Figure 10.** “Magneto-optical sensors” publications and citations made by Web of Science on October 20, 2023 [from Web of Science searching “Magneto-optical sensors”].

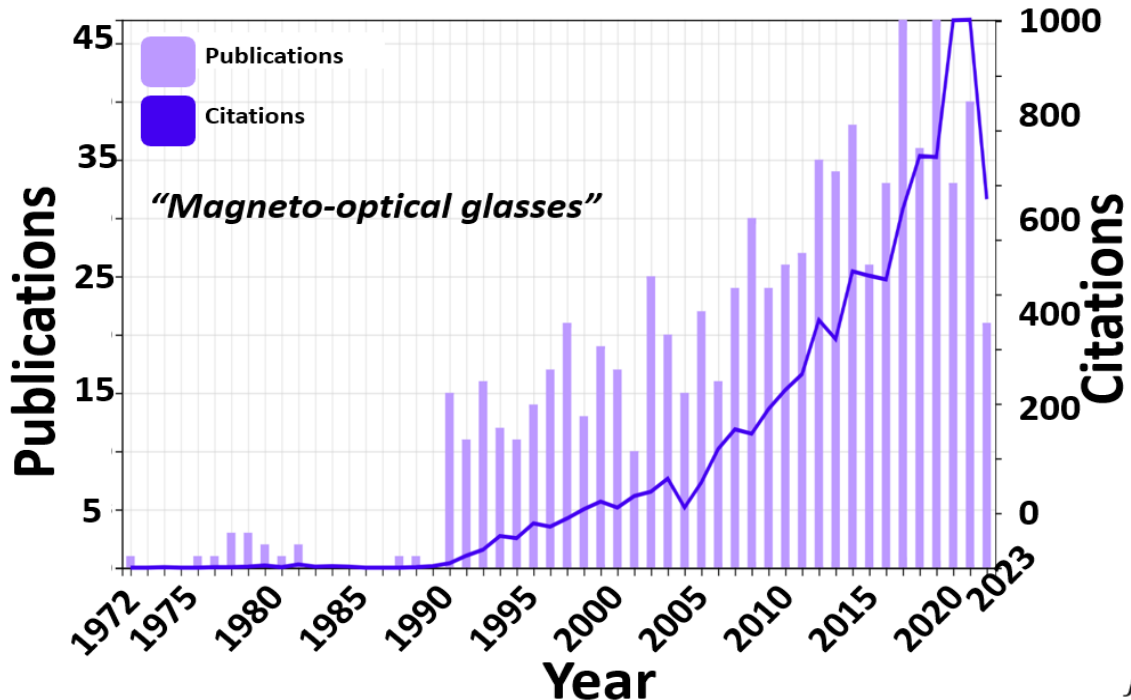


**Figure 11.** “Magneto-optical glasses” publications and citations made by Web of Science on April 14, 2023 [from Web of Science searching “Magneto-optical glasses”].

Several different applications can be mentioned, the main ones being magnetic and electrical sensors, normally made of a copper coil rotating around the MO material, with the coil connected to the electrical circuit. The polarization state of the light propagating in the material is rotated due to the Faraday effect generated by the current passing through the cable. Optical isolators are devices that allow light to pass through in one direction but block it in the opposite direction. They are crucial in many optical systems, such as laser systems, where it is essential to prevent reflections from interfering with the laser's operation. In this application, the MO material is used to rotate the plane of polarized light, which allows the light to pass through the isolator in one direction but blocks it in the opposite direction. Even the Laser Interferometer Gravitational-Wave Observatory (LIGO) used the magneto-optical properties of the TGG during the detection of gravitational waves in 2016[78–80].

MO materials are also used in optical modulators, which are devices that modulate the intensity or phase of light. In this application, the magneto-optical material is used to rotate the plane of polarized light, which changes the intensity or phase of the light passing through it. Optical modulators have several applications, including in fiber-optic communication systems, where they are used to modulate the light signals carrying information.

Another significant application of MO materials is in magnetic field sensors. These sensors are used in various applications, including navigation systems, geophysical exploration, and medical diagnosis. In this application, the magneto-optical material is used to detect and measure magnetic fields. When a magnetic field is applied to the material, it causes a rotation of the plane of polarized light, which can be detected and measured. Figure 12 shows the field values produced by natural events. The sensitivity values of the MO materials are also an important value to know and understand.

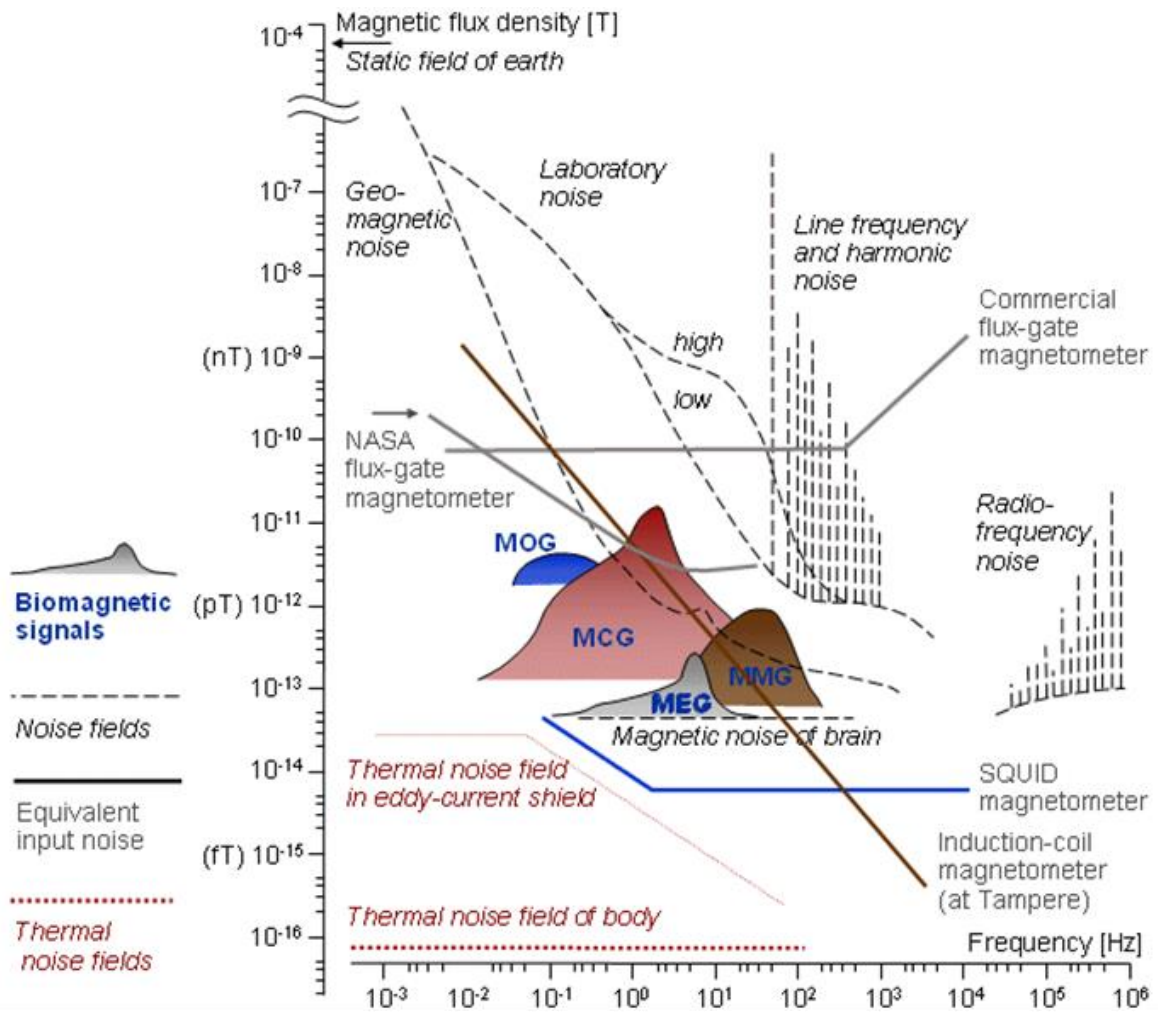


**Figure 12.** Magnetic signals produced by various sources[81].

Another recent spotlight was the improvement of the study of magnetism control using electric field in materials with high magnetic susceptibility, changing the population of charge carriers, paving the way for their use in spintronic integrated circuits with ultra-low energy consumption. Although studies use ferromagnetic carriers, paramagnetic materials also have their relevance, being an area still little studied[82–84].

The MO properties in glasses can be achieved by introducing paramagnetic ions, uniformly incorporated into solid glass matrices is the key to achieving large Faraday rotation through a transparent glassy material. These ions interact with the electromagnetic waves, causing the rotation of the plane of polarized light. The degree of rotation depends on the strength of the magnetic field and the concentration of the magnetic ions in the glass. The main approach to increase the green

constant is to increase the amount of these ions dissolved in the glass matrix, maintaining its optical properties in the region of interest. One of the first works focused on the production of glasses containing rare earths for MO applications is the works by Nicholas Borrelli[69], by the Corning Glass Works, and C. B. Rubinstein et al[85,86], by the Bell Telephone Laboratories, the three works published in 1964. His work demonstrated that the material's  $V$  depended directly on the concentration of RE ions formulated in the final glass. These works also revealed that the  $Tb^{3+}$  ion had the greatest magneto-optical effect, mainly due to its fundamental level and  $J$ .

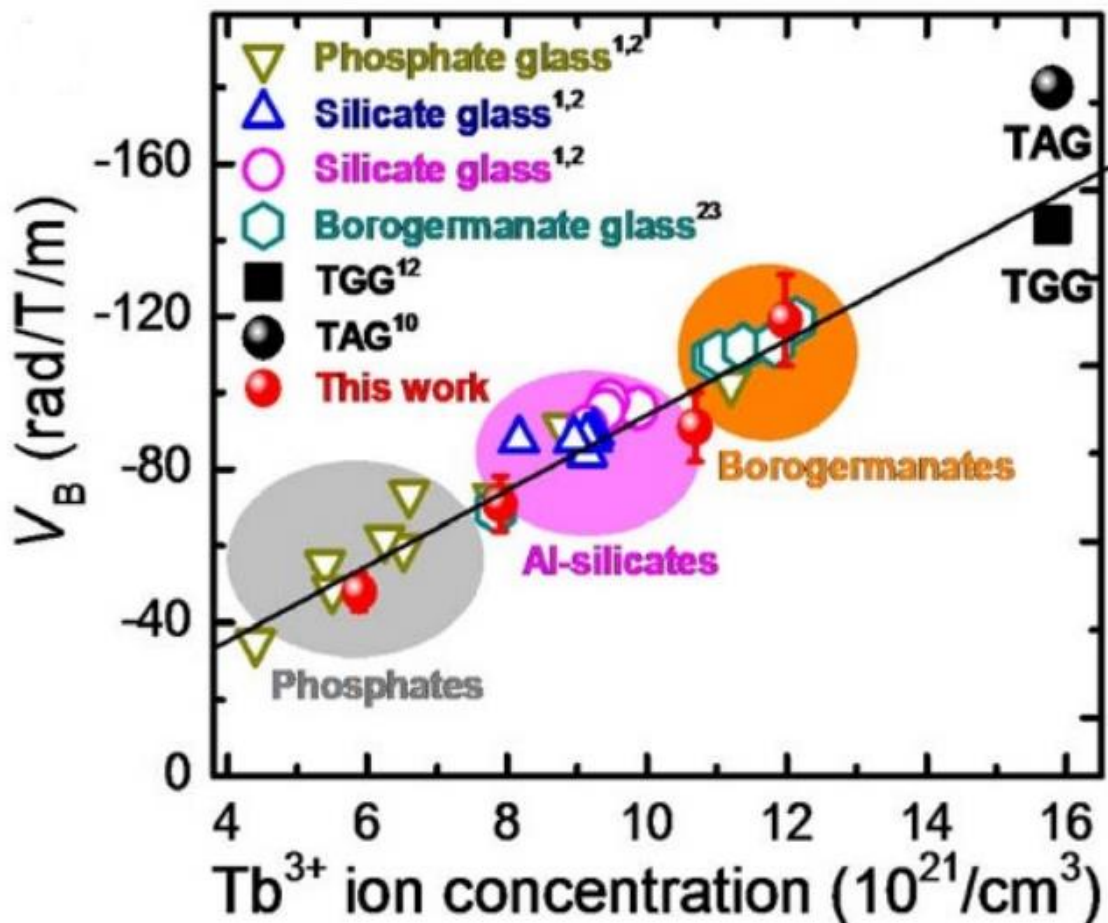


**Figure 13.** Dependence of  $V$  on  $Tb^{3+}$  ion concentration and comparison to other reported data glasses at a fixed wavelength of 632.8 nm [87].

M. Yamane and Y. Asahara[66], and G. Gao et al[87], produced a relation between the  $V$  of some terbium-containing glasses and different matrices by the concentration of  $Tb^{3+}$  ions per volume, at 632.8 nm. Figure 13 is taken from the article

by G. Gao. We observed that phosphate glasses have a lower capacity to dissolve  $Tb^{3+}$  ions, going through silicate and alumino-silicate glasses to borogermanate glasses, with the highest amounts of ions per volume even in so. Germanium also helps with higher  $V$  values because germanium is a polarizable atom, which increases the refractive index of the glass, which is directly proportional to  $V$  as seen earlier.

One of the disadvantages of germanate glasses is their high value ( $\sim$  \$1,600 / 100 g,  $\geq 99.99\%$  trace metals basis, by Sigma-Aldrich), which makes the final product more expensive, which leads us to study one of the systems in this work, changing the germanium for another polarizable atom.

In addition to the germanate glasses, borates[88,89], boro- and aluminosilicates[90–93], phosphates[94–96] glasses also have good solubility of lanthanides, but for good applications in photonics and magneto-optics it will be interesting that the chosen system presents 5 main characteristics: high paramagnetic ions concentration, high refractive index, low absorption coefficient (in the operational spectral region), high thermal stability against devitrification, in order to obtain large bulk samples and eventually optical fibers and a more affordable price than germanate glass.

Borotungstate glasses[97–102], fulfil these requirements, presenting high solubility of  $Ln_2O_3$ , high refractive index (1,6-1,9) due to the higher polarizability of tungsten atoms, besides to be transparent from the visible to near infrared, include the telecom region (1.55  $\mu m$ ). The price of tungsten is also lower than germanate ( $\sim$  \$180 / 100 g, powder, puriss., 99.9%, by Sigma-Aldrich), and the synthesis temperature is lower (1450  $^{\circ}C$  for borogermanate glasses and 1250  $^{\circ}C$  for borotungstate glasses). As stated in the review work by Mohamed Ataalla et al[98], the presence of tungsten in these glasses entails several other interesting characteristics that can be explored, mainly in sensing field, like gas, electric, humidity, light, temperature, high energy radiation sensors, which can lead to more characteristics interesting in the material in future discussions. In addition to  $WO_3$  being a great modifier of the vitreous network, breaking the former chains and allowing greater stability for the vitreous phase. The glass system  $Ln_2O_3$ - $B_2O_3$ - $WO_3$  ( $Ln$  = lanthanide trivalent ion) studied in this work has been

previously explored[103–110], mainly with high concentrations of  $\text{La}^{3+}$  and  $\text{Gd}^{3+}$  glasses.

In this work we will study in depth the  $\text{Ln}_2\text{O}_3\text{-B}_2\text{O}_3\text{-WO}_3$  system for applications in magneto-optics, firstly with trivalent terbium ion ( $\text{Ln}^{3+} = \text{Tb}^{3+}$ ), as this has the highest value of paramagnetic susceptibility of the lanthanides and low absorption in the visible region, making the best glass-forming region effective, improving the parameters of the synthesis process and, subsequently, applying it to other lanthanides.

On the other hand, we can choose to use transition metals (TM) to obtain Faraday rotators. This makes the process even cheaper, as lanthanide ions also have high market values. Fe, Co and Ni ions are already commercially used as Faraday rotators glasses, they have higher V even than glasses containing rare earths, but they are generally used in the infrared region, as they have high absorption in the visible region. In this sense, depending on the need for sensitivity and application, glasses with other TMs that present greater transparency in the visible region, can find specific niches in the market with much more affordable prices.

One of the proposals is the use of divalent manganese ion ( $\text{Mn}^{2+}$ ) as active ion is convenient instead of Fe, Co and Ni, as it is the next ion with greater paramagnetic susceptibility.  $\text{Mn}^{2+}$  is also important due to the extreme sensitivity of its optical spectra in the nature of the host matrix and has been regularly used as a paramagnetic probe (for low grades) in glassy systems.

In glass matrices, manganese can be present in the form of  $\text{Mn}^{2+}$  or  $\text{Mn}^{3+}$  ions, that is,  $d^5$  and  $d^4$ , respectively, occupying tetrahedral and/or octahedral sites depending on the chemical composition. Octahedral  $\text{Mn}^{2+}$  exhibits transparency in the visible window, being limited by the low-intensity prohibited absorption at 410 nm ( ${}^6\text{A}_1(\text{S}) \rightarrow {}^4\text{A}_1, {}^4\text{E}(\text{G})$ ) extending the optical window, compared to magneto-optical glasses containing  $\text{Tb}^{3+}$  (480 nm) . As far as magneto-optical properties are concerned, the use of  $\text{Mn}^{2+}$  is also interesting over all other TMs, as it is the only one that can be loaded in large amounts without compromising the optical absorption window in the visible or infrared. next.

For higher performance of MO material, we need high refractive index. In this sense, a glass composition based on antimony, a highly polarizable ion, which has higher refractive indices and is a well-known matrix for  $Mn^{2+}$  ions, was chosen.

Phosphate glasses generally have low optical dispersion (high Abbe number), large transmission window and high refractive index[111]. The presence of Pb also increases the refractive index of the glass, as already discussed. The addition of PbO and ZnO also lower the melting point of the glass because they are network modifiers, breaking the former interactions.

R. S. Manzan [112,113] and C. A. S. Lereno[114], which this work follows, prepared  $SbPO_4$ -PbO-ZnO glasses doped with Mn and Fe, conferring magnetic properties to them, due to the formation of a glass-ceramic, containing crystals with the ferromagnetic oxides of each mentioned metal. However, the magneto-optical applications of these glasses have not yet been studied, which leads us to this work in question. We had the participation of Scientific Initiation student, Nicole Gouveia Roque, with VUNESP Scholarship, an agreement between the Secretary of Education of the State of São Paulo-UNESP-VUNESP Foundation, who helped in the preparation and study of these glasses.

## References in this chapter

- [1] H. V. Merrick, F.H. Brown, Obsidian sources and patterns of source utilization in Kenya and northern Tanzania: some initial findings, *African Archaeol. Rev.* 2 (1984) 129–152. <https://doi.org/10.1007/BF01117229>.
- [2] J.R. Cann, C. Renfrew, The Characterization of Obsidian and its application to the Mediterranean Region, *Proc. Prehist. Soc.* 30 (1964) 111–133. <https://doi.org/https://doi.org/10.1017/S0079497X00015097>.
- [3] A. Yoshida, Y. Kudo, K. Shimada, J. Hashizume, A. Ono, Impact of landscape changes on obsidian exploitation since the Palaeolithic in the central highland of Japan, *Veg. Hist. Archaeobot.* 25 (2016) 45–55. <https://doi.org/10.1007/s00334-015-0534-y>.
- [4] L.E. Morgan, P.R. Renne, R.E. Taylor, G. WoldeGabriel, Archaeological age constraints from extrusion ages of obsidian: Examples from the Middle Awash, Ethiopia, *Quat. Geochronol.* 4 (2009) 193–203. <https://doi.org/10.1016/j.quageo.2009.01.001>.
- [5] B. Gratuze, Obsidian characterization by laser ablation ICP-MS and its application to prehistoric trade in the Mediterranean and the Near East: Sources and distribution of obsidian within the Aegean and Anatolia, *J. Archaeol. Sci.* 26 (1999) 869–881. <https://doi.org/10.1006/jasc.1999.0459>.
- [6] J.M. Erlandson, T.C. Rick, T.J. Braje, M. Casperson, B. Culleton, B. Fulfrost, T. Garcia, D. a Guthrie, N. Jew, D.J. Kennett, M.L. Moss, L. Reeder, C. Skinner, J. Watts, L. Willis, Paleoindian Seafaring, Maritime Technologies, and Coastal Foraging on California’s Channel Islands, *Science* (80-. ). 331 (2011) 1181–1185. <https://doi.org/10.1126/science.1201477>.
- [7] C. Wilke, The ancient origins of glass, *Knowable Mag.* (2021) 1–12. <https://doi.org/10.1146/knowable-111721-1>.
- [8] A.J. Shortland, M.S. Tite, Raw materials of glass from Amarna and implications for the origins of Egyptian glass, *Archaeometry.* 42 (2000) 141–151. <https://doi.org/10.1111/j.1475-4754.2000.tb00872.x>.
- [9] S. J, Who were the glassmakers? Status, theory and method in mid- second

- millenium glass production., Oxford J. Archaeol. 26 (2007) 261–274.  
<http://onlinelibrary.wiley.com/doi/10.1111/j.1468-0092.2007.00284.x/full>.
- [10] A. Shortland, L. Schachner, I. Freestone, M. Tite, Natron as a flux in the early vitreous materials industry: Sources, beginnings and reasons for decline, J. Archaeol. Sci. 33 (2006) 521–530. <https://doi.org/10.1016/j.jas.2005.09.011>.
- [11] E. V. Sayre, R.W. Smith, Compositional Categories of Ancient Glass, Science (80-. ). 133 (1961) 1824–1826.
- [12] M.S. Walton, A. Shortland, S. Kirk, P. Degryse, Evidence for the trade of Mesopotamian and Egyptian glass to Mycenaean Greece, J. Archaeol. Sci. 36 (2009) 1496–1503. <https://doi.org/10.1016/j.jas.2009.02.012>.
- [13] I. Freestone, N. Meeks, M. Sax, C. Higgitt, The Lycurgus Cup - A Roman nanotechnology, Gold Bull. 40 (2008) 270–277. <https://doi.org/10.1007/BF03215599>.
- [14] G.W. Morey, Optical glasses, 2150694, 1936. <https://doi.org/10.1038/209966a0>.
- [15] B.T. Kolomiets, Vitreous Semiconductors, Pliys. Stat. Sol. 7 (1964) 359–372.
- [16] W. Klement, R.H. Willens, P. Duwez, Non-crystalline structure in solidified gold-silicon alloy, Nature. 187 (1960) 869–870.
- [17] E. Snitzer, Optical maser action of  $\text{Nd}^{+3}$  in a barium crown glass, Phys. Rev. Lett. 7 (1961) 444–446. <https://doi.org/10.1103/PhysRevLett.7.444>.
- [18] M. Poulain, M. Poulain, J. Lucas, Verres fluores au tetrafluorure de zirconium proprietes optiques d'un verre dope au  $\text{Nd}^{3+}$ , Mater. Res. Bull. 10 (1975) 243–246.
- [19] C.C. Kao, G.A. Hockham, Dielectric-fibre surface waveguides for optical frequencies, Proc. IEE. 113 (1966) 1151–1158. <https://doi.org/10.1049/piee.1966.0189>.
- [20] W. Blanc, Y. Gyu Choi, X. Zhang, M. Nalin, K.A. Richardson, G.C. Righini, M. Ferrari, A. Jha, J. Massera, S. Jiang, J. Ballato, L. Petit, The past, present and future of photonic glasses: A review in homage to the United Nations International Year of glass 2022, Prog. Mater. Sci. 134 (2023) 101084. <https://doi.org/10.1016/j.pmatsci.2023.101084>.
- [21] T. Bajarin, Why Glass Is Critical to the Future of Tech, Recode.Net. (2015)

- <http://www.recode.net/2015/12/14/11621456/why-glas>.
- [22] A. Durán, J.M. Parker, Welcome to the Glass Age. Celebrating the United Nations International Year of Glass 2022, CSIC, 2022.
- [23] D.L. Morse, J.W. Evenson, Welcome to the Glass Age, *Int. J. Appl. Glas. Sci.* 7 (2016) 409–412. <https://doi.org/10.1111/ijag.12242>.
- [24] M. Faraday, I. The Bakerian Lecture.— On the manufacture of glass for optical purposes, *Philos. Trans. R. Soc. London.* 120 (1830) 1–57. <https://doi.org/10.1098/rstl.1830.0002>.
- [25] G. Tammann, Ueber die Kristallisationsgeschwindigkeit, II. *Z. Phys. Chem.* 26 (1898) 307–316.
- [26] G. Tammann, Glasses as supercooled liquids, *J. Soc. Glas. Technol.* 9 (1925) 166–185.
- [27] W. L. Bragg, Atomic Structure of Minerals, *J. Phys. Chem.* 41 (1937) 1149–1150. <https://doi.org/10.1021/j150386a017>.
- [28] J.T. Randall, H.P. Rooksby, B.S. Cooper, X-ray diffraction and the structure of vitreous silica, *Z. Krist.* 75 (1930) 196–214.
- [29] R.W.G. Wyckoff, G.W. Morey, X-ray diffraction measurement of some soda-lime-silica glasses, *J. Soc. Glas. Technol.* 9 (1925) 265–267.
- [30] A.A. Lebedev, The polymorphism and annealing of glass, *Trans. Opt. Inst. Petrograd.* 2 (1921) 1–20.
- [31] W.H. Zachariasen, The Atomic arrangement in Glass, *J. Am. Chem. Soc.* 196 (1932) 3841–3851. <https://doi.org/10.1021/ja01349a006>.
- [32] P.Y. Huang, S. Kurasch, A. Srivastava, V. Skakalova, J. Kotakoski, A. V. Krashennnikov, R. Hovden, Q. Mao, J.C. Meyer, J. Smet, D.A. Muller, U. Kaiser, Direct Imaging the Atoms in a Two-Dimensional Silica Glass on Graphene, *Microsc. Microanal.* 18 (2012) 1496–1497. <https://doi.org/10.1017/S1431927612009336>.
- [33] M. Heyde, S. Shaikhutdinov, H.J. Freund, Two-dimensional silica: Crystalline and vitreous, *Chem. Phys. Lett.* 550 (2012) 1–7. <https://doi.org/10.1016/j.cplett.2012.08.063>.
- [34] J. Wong, C.A. Angell, *Glass: structure by spectroscopy*, University Microfilms,

- 1976.
- [35] S. R. Elliott, *Physics of amorphous materials*, Essex: Lon, 1989.
- [36] J. (Université de M.I. Zarzycki, *Glasses and the Vitreous State*, Cambridge University Press, 1991.
- [37] R.H. Doremus, *Glass Science*, 2nd ed., Wiley-Interscience, 1994.
- [38] E.D. Zanotto, Do cathedral glasses flow?, *Am. J. Phys.* 66 (1998) 392–395. <https://doi.org/10.1119/1.19026>.
- [39] J.E. Shelby, *Introduction to Glass Science and Technology*, The Royal Society of Chemistry, 1997. <https://doi.org/10.1039/9781847551160>.
- [40] P. K. Gupta, Non-crystalline solids: glasses and amorphous solids, *J. Non-Cryst. Solids.* 195 (1996) 158–164. [https://doi.org/10.1016/0022-3093\(95\)00502-1](https://doi.org/10.1016/0022-3093(95)00502-1).
- [41] O.L. Alves, I. de F. Gimenez, I.O. Mazali, *Vidros*, *Química Nov. Na Esc. Edição Esp* (2001) 13–24.
- [42] A.K. Varshneya, J.C. Mauro, *Fundamentals of Inorganic Glasses*, 3rd ed., Elsevier, 2019.
- [43] E.D. Zanotto, J.C. Mauro, The glassy state of matter: Its definition and ultimate fate, *J. Non. Cryst. Solids.* 471 (2017) 490–495. <https://doi.org/10.1016/j.jnoncrysol.2017.05.019>.
- [44] P.I.K. Onorato, D.R. Uhlmann, Nucleating heterogeneities and glass formation, *J. Non-Cryst. Sol.* 22 (1976) 367–378. [https://doi.org/10.1016/0022-3093\(76\)90066-1](https://doi.org/10.1016/0022-3093(76)90066-1).
- [45] R. Elliott, The story of magnetism, *Physica A.* 384 (2007) 44–52.
- [46] J. M. D. Coey, Magnetism in future, *J. Magn. Magn. Mater.* 226 (2001) 2107–2112.
- [47] J.M.D. (Trinity C.D. Coey, *Magnetism and Magnetic Materials*, Cambridge University Press, Cambridge, 2010.
- [48] G. Cantor, *Michael Faraday: Sandemanian and Scientist*, Palgrave Macmillan London, 1991. <https://doi.org/https://doi.org/10.1007/978-1-349-13131-0>.
- [49] M. Faraday, I. Experimental researches in electricity.—Nineteenth series, *Philos. Trans. R. Soc. London.* 136 (1846) 1–20. <https://doi.org/10.1098/rstl.1846.0001>.
- [50] M. Faraday, *Faraday’s Diary of Experimental Investigation, 1820-1862, 7 Vol.,*

- 1936.
- [51] J. Kerr, XLIII. On rotation of the plane of polarization by reflection from the pole of a magnet, *Philos. Mag.* 3 (1877) 321–343. <https://doi.org/10.1080/14786447708639245>.
- [52] J. Kerr, XXIV. On reflection of polarized light from the equatorial surface of a magnet, *Philos. Mag.* 5 (1878) 161–177. <https://doi.org/10.1080/14786447808639407>.
- [53] H. Ebert, Magneto-optical effects in transition metal systems, *Reports Prog. Phys.* 59 (1996) 1665–1735. <https://doi.org/10.1088/0034-4885/59/12/003>.
- [54] M.J. Freiser, A Survey of Magneto-Optic Effects, *IEEE Trans Mag.* 4 (1968) 152–161.
- [55] V. Rodriguez, D. Verreault, F. Adamietz, A. Kalafatis, All-Optical Measurements of the Verdet Constant in Achiral and Chiral Liquids: Toward All-Optical Magnetic Spectroscopies, 2022. <https://doi.org/10.1021/acsp Photonics.2c00720>.
- [56] P. Pascal, No Title, *Ann. Chim. Phys.* 19 (1910) 5.
- [57] P. Pascal, No, *Ann. Chim. Phys.* 25 (1912) 289.
- [58] P. Pascal, No Title, *Ann. Chim. Phys.* 28 (1913) 218.
- [59] G.A. Bain, J.F. Berry, Diamagnetic corrections and Pascal's constants, *J. Chem. Educ.* 85 (2008) 532–536. <https://doi.org/10.1021/ed085p532>.
- [60] Pierre Curie, Propriétés magnétiques des corps à diverses températures, *Faculté des Sciences de Paris*, 1895.
- [61] P.-E. Weiss, G. Foëx, *Le Magnétisme*, 1926.
- [62] R.S. Yadav, Anju, T. Jamatia, I. Kuřitka, J. Vilčáková, D. Škoda, P. Urbánek, M. Machovský, M. Masař, M. Urbánek, L. Kalina, J. Havlica, Superparamagnetic znfe<sub>2</sub>o<sub>4</sub> nanoparticles-reduced graphene oxide-polyurethane resin based nanocomposites for electromagnetic interference shielding application, *Nanomaterials*. 11 (2021). <https://doi.org/10.3390/nano11051112>.
- [63] V. Marghussian, Magnetic Properties of Nano-Glass Ceramics, in: V. Marghussian (Ed.), *Nano-Glass Ceram.*, William Andrew Publishing, 2015: pp. 181–223. <https://doi.org/10.1016/B978-0-323-35386-1.00004-9>.
- [64] M. Krnel, S. Vrtnik, A. Jelen, P. Koželj, Z. Jagličić, A. Meden, M. Feuerbacher,

- J. Dolinšek, Speromagnetism and asperomagnetism as the ground states of the Tb-Dy-Ho-Er-Tm “ideal” high-entropy alloy, *Intermetallics*. 117 (2020). <https://doi.org/10.1016/j.intermet.2019.106680>.
- [65] H. Yang, Z. Zhu, Magneto-optical glass mixed with Tb<sup>3+</sup> ions: High Verdet constant and luminescence properties, *J. Lumin.* 231 (2021) 117804. <https://doi.org/10.1016/j.jlumin.2020.117804>.
- [66] M. Yamane, Y. Asahara, *Glasses for Photonics*, Cambridge University Press, Cambridge, 2000.
- [67] H. Becquerel, No Title, *Compt. Rend.* 125 (1897).
- [68] J.H. Van Vleck, M.H. Hebb, On the paramagnetic rotation of tysonite, *Phys. Rev.* 46 (1934) 17–32. <https://doi.org/10.1103/PhysRev.46.17>.
- [69] N.F. Borrelli, Faraday rotation in glasses, *J. Chem. Phys.* 41 (1964) 3289–3293. <https://doi.org/10.1063/1.1725727>.
- [70] M. Valeanu, M. Sofronie, A.C. Galca, F. Tolea, M. Elisa, B. Sava, L. Boroica, V. Kuncser, The relationship between magnetism and magneto-optical effects in rare earth doped aluminophosphate glasses, *J. Phys. D. Appl. Phys.* 49 (2016). <https://doi.org/10.1088/0022-3727/49/7/075001>.
- [71] O. Louant, V. Liégeois, T. Verbiest, A. Persoons, B. Champagne, Faraday Effect in Stacks of Aromatic Molecules, *J. Phys. Chem. C*. 121 (2017) 15348–15352. <https://doi.org/10.1021/acs.jpcc.7b04177>.
- [72] S. Vandendriessche, S. Van Cleuvenbergen, P. Willot, G. Hennrich, M. Srebro, V.K. Valev, G. Koeckelberghs, K. Clays, J. Autschbach, T. Verbiest, Giant faraday rotation in mesogenic organic molecules, *Chem. Mater.* 25 (2013) 1139–1143. <https://doi.org/10.1021/cm4004118>.
- [73] C.-K. Lim, M.J. Cho, A. Singh, Q. Li, W.J. Kim, H.S. Jee, K.L. Fillman, S.H. Carpenter, M.L. Neidig, A. Baev, M.T. Swihart, P.N. Prasad, Manipulating Magneto-Optic Properties of a Chiral Polymer by Doping with Stable Organic Biradicals, *Nano Lett.* 16 (2016) 5451–5455. <https://doi.org/10.1021/acs.nanolett.6b01874>.
- [74] K.J. Carothers, N.P. Lyons, N.G. Pavlopoulos, K.S. Kang, T.M. Kochenderfer, A. Phan, L.N. Holmen, S.L. Jenkins, I.B. Shim, R.A. Norwood, J. Pyun, *Polymer-*

- coated magnetic nanoparticles as ultrahigh verdet constant materials: Correlation of nanoparticle size with magnetic and magneto-optical properties, *Chem. Mater.* 33 (2021) 5010–5020. <https://doi.org/10.1021/acs.chemmater.1c00808>.
- [75] S. Ganschow, D. Klimm, P. Reiche, R. Uecker, On the Crystallization of Terbium Aluminium Garnet, *Cryst. Res. Technol.* 34 (1999) 615–619.
- [76] M. Geho, T. Sekijima, T. Fujii, Growth of terbium aluminum garnet ( $\text{Tb}_3\text{Al}_5\text{O}_{12}$ ; TAG) single crystals by the hybrid laser floating zone machine, *J. Cryst. Growth.* 267 (2004) 188–193. <https://doi.org/10.1016/j.jcrysgr.2004.03.068>.
- [77] D. Vojna, O. Slezák, A. Lucianetti, T. Mocek, Verdet constant of magneto-active materials developed for high-power Faraday devices, *Appl. Sci.* 9 (2019). <https://doi.org/10.3390/app9153160>.
- [78] T.L.S. Collaboration, Advanced LIGO, *Class. Quantum Gravity.* 32 (2015). <https://doi.org/10.1088/0264-9381/32/7/074001>.
- [79] O. V. Palashov, D.S. Zheleznov, A. V. Voitovich, V. V. Zelenogorsky, E.E. Kamenetsky, E.A. Khazanov, R.M. Martin, K.L. Dooley, L. Williams, A. Lucianetti, V. Quetschke, G. Mueller, D.H. Reitze, D.B. Tanner, E. Genin, B. Canuel, J. Marque, High-vacuum-compatible high-power Faraday isolators for gravitational-wave interferometers, *J. Opt. Soc. Am. B.* 29 (2012) 1784. <https://doi.org/10.1364/josab.29.001784>.
- [80] The LIGO Scientific Collaboration, Observation of gravitational waves from a binary black hole merger, *Phys. Rev. Lett.* 116 (2016) 1–16. <https://doi.org/10.1103/PhysRevLett.116.061102>.
- [81] J. Malmivuo, R. Plonsey, Theory of Biomagnetic Measurements, in: *Bioelectromagn. Princ. Appl. Bioelectric Biomagn. Fields*, Oxford University Press, 1995: pp. 325–363.
- [82] F. Matsukura, Y. Tokura, H. Ohno, Control of magnetism by electric fields, *Nat. Nanotechnol.* 10 (2015) 209–220. <https://doi.org/10.1038/nnano.2015.22>.
- [83] C. Song, Y. You, X. Chen, X. Zhou, Y. Wang, F. Pan, How to manipulate magnetic states of antiferromagnets, *Nanotechnology.* 29 (2018). <https://doi.org/10.1088/1361-6528/aaa812>.
- [84] G. Assefa, Electric Field Controlled Itinerant Carrier Spin Polarization in

- Ferromagnetic Semiconductors, *Adv. Condens. Matter Phys.* 2021 (2021).  
<https://doi.org/10.1155/2021/6663876>.
- [85] C.B. Rubinstein, S.B. Berger, L.G. Van Uitert, W.A. Bonner, Faraday rotation of rare-earth (III) borate glasses, *J. Appl. Phys.* 35 (1964) 2338–2340.  
<https://doi.org/10.1063/1.1702860>.
- [86] C.B. Rubinstein, L.G. Van Uitert, W.H. Grodkiewicz, Magneto-optical properties of rare earth (III) aluminum garnets, *J. Appl. Phys.* 35 (1964) 3069–3070.  
<https://doi.org/10.1063/1.1713182>.
- [87] G. Gao, A. Winterstein-Beckmann, O. Surzhenko, C. Dubs, J. Dellith, M.A. Schmidt, L. Wondraczek, Faraday rotation and photoluminescence in heavily Tb<sup>3+</sup>-doped GeO<sub>2</sub>-B<sub>2</sub>O<sub>3</sub>-Al<sub>2</sub>O<sub>3</sub>-Ga<sub>2</sub>O<sub>3</sub> glasses for fiber-integrated magneto-optics, *Sci. Rep.* 5 (2015) 1–6. <https://doi.org/10.1038/srep08942>.
- [88] M. Zagrai, M. Unguresan, S. Rada, J. Zhang, M. Pica, E. Culea, Local structure in gadolinium-lead-borate glasses and glass-ceramics, *J. Non. Cryst. Solids.* 546 (2020) 120259. <https://doi.org/10.1016/j.jnoncrysol.2020.120259>.
- [89] S. Sasaki, A. Masuno, K. Ohara, Y. Yanaba, H. Inoue, Y. Watanabe, S. Kohara, Structural Origin of Additional Infrared Transparency and Enhanced Glass-Forming Ability in Rare-Earth-Rich Borate Glasses without B-O Networks, *Inorg. Chem.* 59 (2020) 13942–13951. <https://doi.org/10.1021/acs.inorgchem.0c01567>.
- [90] H. Yin, Y. Gao, H. Guo, C. Wang, C. Yang, Effect of B<sub>2</sub>O<sub>3</sub> Content and Microstructure on Verdet Constant of Tb<sub>2</sub>O<sub>3</sub>-Doped GBSG Magneto-Optical Glass, *J. Phys. Chem. C.* 122 (2018) 16894–16900.  
<https://doi.org/10.1021/acs.jpcc.8b04989>.
- [91] H. Lin, H. Yang, L. Zhou, J. He, B. Liu, N. Li, C. Li, S. Li, W. Yang, X. Jiang, H. Liu, F. Zeng, Z. Su, Research on the physical and optical properties of Dy<sub>3+</sub> doped 30 mol% Tb<sub>2</sub>O<sub>3</sub>-B<sub>2</sub>O<sub>3</sub>-GeO<sub>2</sub>-PbO-SiO<sub>2</sub> magneto-optical glass with high verdet constant, *J. Phys. Chem. Solids.* 166 (2022) 110682.  
<https://doi.org/10.1016/J.JPCS.2022.110682>.
- [92] S. Ju, J. Kim, K. Linganna, P.R. Watekar, S.G. Kang, B.H. Kim, S. Boo, Y. Lee, Y.H. An, C.J. Kim, W.T. Han, Temperature and vibration dependence of the faraday effect of Gd<sub>2</sub>O<sub>3</sub> NPs-doped alumino-silicate glass optical fiber, *Sensors*

- (Switzerland). 18 (2018) 1–13. <https://doi.org/10.3390/s18040988>.
- [93] V.D. Dubrovin, X. Zhu, M. Mollaei, J. Zong, N. Peyghambarian, Highly Dy<sub>2</sub>O<sub>3</sub> and Er<sub>2</sub>O<sub>3</sub> doped boron-aluminosilicate glasses for magneto-optical devices operating at 2 μm, *J. Non. Cryst. Solids.* 569 (2021) 120986. <https://doi.org/10.1016/J.JNONCRY SOL.2021.120986>.
- [94] M. Elisa, R. Stefan, I.C. Vasiliu, M.I. Rusu, B.A. Sava, L. Boroica, M. Sofronie, V. Kuncser, A.C. Galca, A. Beldiceanu, A. Volceanov, M. Eftimie, Thermal, structural, magnetic and magneto-optical properties of dysprosium-doped phosphate glass, *J. Non. Cryst. Solids.* 521 (2019) 119545. <https://doi.org/10.1016/J.JNONCRY SOL.2019.119545>.
- [95] B. Bellanger, Y. Ledemi, Y. Messaddeq, Fluorophosphate Glasses with High Terbium Content for Magneto-optical Applications, *J. Phys. Chem. C.* 124 (2020) 5353–5362. <https://doi.org/10.1021/acs.jpcc.9b11696>.
- [96] A. Babkina, E. Kulpina, Y. Sgibnev, Y. Fedorov, A. Starobor, O. Palashov, N. Nikonorov, A. Ignatiev, K. Zyryanova, K. Oreshkina, E. Zhizhin, D. Pudikov, Terbium concentration effect on magneto-optical properties of ternary phosphate glass, *Opt. Mater. (Amst).* 100 (2020) 109692. <https://doi.org/10.1016/j.optmat.2020.109692>.
- [97] R.M. Abdelouhab, R. Braunstein, K. Bärner, Identification of tungstate complexes in lithium-tungstate-borate glasses by Raman spectroscopy, *J. Non. Cryst. Solids.* 108 (1989) 109–114. [https://doi.org/10.1016/0022-3093\(89\)90338-4](https://doi.org/10.1016/0022-3093(89)90338-4).
- [98] M. Ataalla, A.S. Afify, M. Hassan, M. Abdallah, M. Milanova, H.Y. Aboul-Enein, A. Mohamed, Tungsten-based glasses for photochromic, electrochromic, gas sensors, and related applications: A review, *J. Non. Cryst. Solids.* 491 (2018) 43–54. <https://doi.org/10.1016/j.jnoncrysol.2018.03.050>.
- [99] Y. Taki, K. Shinozaki, T. Honma, T. Komatsu, L. Aleksandrov, R. Iordanova, Coexistence of nano-scale phase separation and micro-scale surface crystallization in Gd<sub>2</sub>O<sub>3</sub>-WO<sub>3</sub>-B<sub>2</sub>O<sub>3</sub> glasses, *J. Non. Cryst. Solids.* 381 (2013) 17–22. <https://doi.org/10.1016/j.jnoncrysol.2013.09.014>.
- [100] W. Rittisut, N. Wantana, Y. Ruangtaweep, P. Mool-am-kha, J. Padchasri, S.

- Rujirawat, P. Manyum, R. Yimnirun, P. Kidkhunthod, A. Prasatkhetragarn, S. Kothan, H.J. Kim, J. Kaewkhao, Bright white light emission from (Gd<sup>3+</sup> /Dy<sup>3+</sup>) dual doped transparent lithium aluminum borate glasses for W- LED application, *Opt. Mater. (Amst)*. 122 (2021) 111705. <https://doi.org/10.1016/j.optmat.2021.111705>.
- [101] L. Aleksandrov, T. Komatsu, K. Shinozaki, T. Honma, R. Iordanova, Structure of MoO<sub>3</sub>-WO<sub>3</sub>-La<sub>2</sub>O<sub>3</sub>-B<sub>2</sub>O<sub>3</sub> glasses and crystallization of LaMo<sub>1-x</sub>W<sub>x</sub>BO<sub>6</sub> solid solutions, *J. Non. Cryst. Solids*. 429 (2015) 171–177. <https://doi.org/10.1016/j.jnoncrysol.2015.09.004>.
- [102] Y. Wang, T. Honma, T. Komatsu, Effects of WO<sub>3</sub> substitution on crystallization behavior and laser patterning in Gd<sub>2</sub>O<sub>3</sub>-MoO<sub>3</sub>-B<sub>2</sub>O<sub>3</sub> glasses, *J. Non. Cryst. Solids*. 383 (2014) 86–90. <https://doi.org/10.1016/j.jnoncrysol.2013.04.016>.
- [103] N. Wantana, E. Kaewnuam, Y. Ruangtaweep, D. Valiev, S. Stepanov, K. Yamanoi, H.J. Kim, S. Kothan, J. Kaewkhao, Tunable orange, yellow and white emission of Pr<sup>3+</sup>-doped tungsten gadolinium borate glasses, *J. Non. Cryst. Solids*. 554 (2021) 120603. <https://doi.org/10.1016/j.jnoncrysol.2020.120603>.
- [104] N. Wantana, Y. Ruangtaweep, E. Kaewnuam, S.C. Kang, H.J. Kim, S. Kothan, J. Kaewkhao, Development of WO<sub>3</sub>-Gd<sub>2</sub>O<sub>3</sub>- B<sub>2</sub>O<sub>3</sub> high density glasses doped with Dy<sup>3+</sup> for photonics and scintillation materials application, *Solid State Sci.* 101 (2020) 106135. <https://doi.org/10.1016/j.solidstatesciences.2020.106135>.
- [105] N. Wantana, E. Kaewnuam, Y. Ruangtaweep, D. Valiev, S. Stepanov, K. Yamanoi, H.J. Kim, J. Kaewkhao, Radio, cathodo and photoluminescence investigations of high density WO<sub>3</sub>-Gd<sub>2</sub>O<sub>3</sub>-B<sub>2</sub>O<sub>3</sub> glass doped with Tb<sup>3+</sup>, *Radiat. Phys. Chem.* 164 (2019) 108350. <https://doi.org/10.1016/j.radphyschem.2019.108350>.
- [106] N. Wantana, E. Kaewnuam, Y. Ruangtaweep, P. Kidkhunthod, H.J. Kim, S. Kothan, J. Kaewkhao, High density tungsten gadolinium borate glasses doped with Eu<sup>3+</sup> ion for photonic and scintillator applications, *Radiat. Phys. Chem.* 172 (2020) 108868. <https://doi.org/10.1016/j.radphyschem.2020.108868>.
- [107] N. Wantana, E. Kaewnuam, H.J. Kim, S.C. Kang, Y. Ruangtaweep, S. Kothan, J. Kaewkhao, X-ray/proton and photoluminescence behaviors of Sm<sup>3+</sup> doped high-

- density tungsten gadolinium borate scintillating glass, *J. Alloys Compd.* 849 (2020) 156574. <https://doi.org/10.1016/j.jallcom.2020.156574>.
- [108] R. Iordanova, M. Milanova, L. Aleksandrov, K. Shinozaki, T. Komatsu, Structural study of  $\text{WO}_3\text{-La}_2\text{O}_3\text{-B}_2\text{O}_3\text{-Nb}_2\text{O}_5$  glasses, *J. Non. Cryst. Solids.* 543 (2020) 120132. <https://doi.org/10.1016/j.jnoncrysol.2020.120132>.
- [109] M. Milanova, K.L. Kostov, R. Iordanova, L. Aleksandrov, A. Yordanova, T. Mineva, Local structure, connectivity and physical properties of glasses in the  $\text{B}_2\text{O}_3\text{-Bi}_2\text{O}_3\text{-La}_2\text{O}_3\text{-WO}_3$  system, *J. Non. Cryst. Solids.* 516 (2019) 35–44. <https://doi.org/10.1016/j.jnoncrysol.2019.04.028>.
- [110] L. Aleksandrov, T. Komatsu, R. Iordanova, Y. Dimitriev, Raman spectroscopic study of structure of  $\text{WO}_3\text{La}_2\text{O}_3\text{B}_2\text{O}_3$  glasses with no color and crystallization of  $\text{LaBWO}_6$ , *Opt. Mater. (Amst.)* 34 (2011) 201–206. <https://doi.org/10.1016/j.optmat.2011.08.002>.
- [111] A. Winterstein, H. Akamatsu, D. Möncke, K. Tanaka, M.A. Schmidt, L. Wondraczek, Magnetic and magneto-optical quenching in  $(\text{Mn}^{2+}, \text{Sr}^{2+})$  metaphosphate glasses, *Opt. Mater. Express.* 3 (2013) 184. <https://doi.org/10.1364/ome.3.000184>.
- [112] Renata Siqueira Manzan, *Preparação de Vidros e Vitrocerâmicas no sistema  $\text{SbPO}_4\text{-PbO-ZnO}$  dopados com manganês e ferro*, UFSCar, 2014.
- [113] R.S. Manzan, J.P. Donoso, C.J. Magon, I.D.A.A. Silva, C. Rüssel, M. Nalin, Optical and structural studies of  $\text{Mn}^{2+}$  doped  $\text{SbPO}_4\text{-ZnO-PbO}$  glasses, *J. Braz. Chem. Soc.* 26 (2015) 2607–2614. <https://doi.org/10.5935/0103-5053.20150289>.
- [114] C.A.S. Lereno, *Estudo da cristalização de vidros contendo  $\text{Fe}_2\text{O}_3$  e sua influência nas propriedades ópticas e magneto-ópticas*, IQ-UNESP, 2018.

**CHAPTER VI – Final Conclusion and**  
**Perspectives**

## Chapter VI – Final Conclusion and Perspectives

As general conclusions of this work we can highlight the obtention of two different glass systems presenting magneto optical properties. The borotungstate system showed very high solubility of rare earth ions, which is the pre-requisite to obtain large magneto optical properties and it was demonstrated by the high values of Verdet constant. These glasses present also good thermal stability allowing to prepare large bulk samples. The system containing manganese also showed good magneto optical properties, but, as expected, due to lower magnetic susceptibility of Mn ions, the Verdet constant is lower than that of borotungstate system. In parallel to the main study of this thesis, a series of samples containing different rare earths were produced and studied, the qualitative results indicates that most of them can be used for more specific magneto optical studies while others do not form glasses. The comprehension of such systems is fundamental to advance towards to chipper and more powerful devices.

Our investigation into the physical principles underlying Faraday effects has shed light on the intricate interaction between magnetic fields and these glassy systems, making correlations between glass composition and desired effects to optimize the magneto-optical performance of these glasses. These insights serve as a foundation for the development of advanced optical devices such as magneto-optical modulators and sensors, leveraging the unique properties of these glasses for real-world applications. Looking to the future, the exploration of magneto-optical glasses in borotungstate systems offers interesting prospects for future research. A cheaper matrix that offers an effect comparable to borogermanates and commercial single crystals. Glasses containing manganese also open doors for the development of this and other matrices with transition metals, since the effect can be compared to certain matrices containing lanthanides. In conclusion, the investigation of magneto-optical glasses within specific vitreous systems revealed a range of possibilities for the advancement of optical technologies. The synthesis, characterization, and manipulation of magneto-optical properties within these glasses provide a strong foundation for future research endeavors that aim to push the boundaries of photonics, catalyze innovation, and shape the landscape of modern optical devices.